cmgh
CELLULAR AND MOLECULAR GASTROENTEROLOGY AND HEPATOLOGY

ORIGINAL RESEARCH

Dysfunctional Extracellular Matrix Remodeling Supports Perianal Fistulizing Crohn's Disease by a Mechanoregulated Activation of the Epithelial-to-Mesenchymal Transition

Giulia Rizzo,[1,*] Federica Rubbino,[2,*] Sudharshan Elangovan,[3,*] Giusy Sammarco,[4] Sara Lovisa,[1,4] Silvia Restelli,[1] Samuel Elias Pineda Chavez,[1] Luca Massimino,[5,6] Luigi Lamparelli,[4] Marianna Paulis,[8,9] Annalisa Maroli,[10] Giulia Roda,[4] Mohammad Shalaby,[4] Michele Carvello,[1,10] Caterina Foppa,[10] Sheona P. Drummond,[11] Paola Spaggiari,[12] Federica Ungaro,[5,6,7] Antonino Spinelli,[1,10] Alberto Malesci,[5,7] Alessandro Repici,[1,13] Anthony J. Day,[11,14] Alessandro Armuzzi,[1,4] Silvio Danese,[5,6,7] and Stefania Vetrano[1,4]

[1]Department of Biomedical Sciences, Humanitas University, Pieve Emanuele, Italy; [2]Laboratory of Molecular Gastroenterology, Department of Gastroenterology, IRCCS Humanitas Research Hospital, Rozzano, Italy; [3]Genomics Division, Wipro Life Sciences Lab, Wipro Limited, Bengaluru, India; [4]IBD Unit, Department of Gastroenterology, IRCCS Humanitas Research Hospital, Rozzano, Italy; [5]Department of Gastroenterology and Digestive Endoscopy, IRCCS Ospedale San Raffaele, Milan, Italy; [6]Division of Immunology, Transplantation and Infectious Disease, IRCCS Ospedale San Raffaele, Milan, Italy; [7]Faculty of Medicine, Università Vita-Salute San Raffaele, Milan, Italy; [8]IRCCS Humanitas Research Hospital, Rozzano, Milan, Italy; [9]Institute of Genetic and Biomedical Research, UOS Milan, National Research Council of Italy, Milan, Italy; [10]Colon and Rectal Surgery Unit, IRCCS Humanitas Research Hospital, Rozzano, Italy; [11]Wellcome Centre for Cell-Matrix Research, Faculty of Biology, Medicine and Health, Manchester Academic Health Science Centre, University of Manchester, Manchester, United Kingdom; [12]Department of Pathology, IRCCS Humanitas Research Hospital, Rozzano, Italy; [13]Digestive Endoscopy Unit, Department of Gastroenterology, IRCCS Humanitas Clinical and Research Center, Rozzano, Italy; and [14]Lydia Becker Institute of Immunology and Inflammation, Faculty of Biology, Medicine, and Health, Manchester Academic Health Science Centre, University of Manchester, Manchester, United Kingdom

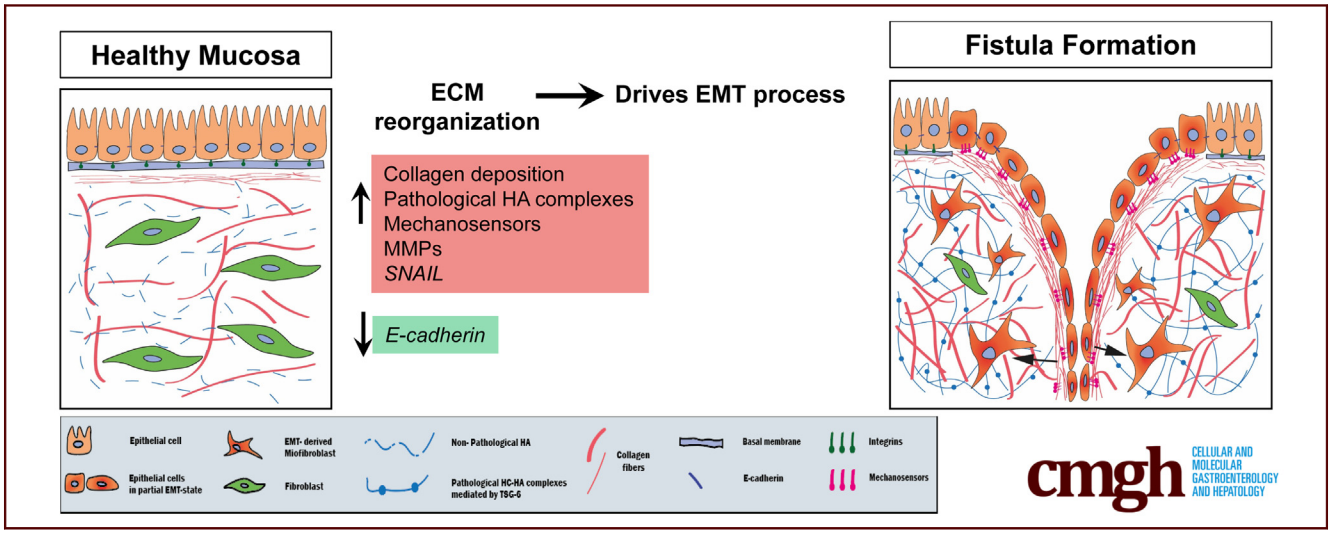

SUMMARY

Perianal fistula is disabling manifestation of Crohn's disease of unknown etiopathogenesis. This study shows that in the fistula area the pathological extracellular matrix organization mediated by TNF-stimulated gene-6 triggers epithelial–mesenchymal transition processes and paves the way for new targets for the treatment of perianal fistula.

BACKGROUND AND AIMS: Perianal fistula represents one of the most disabling manifestations of Crohn's disease (CD) due to complete destruction of the affected mucosa, which is replaced by granulation tissue and associated with changes in tissue organization. To date, the molecular mechanisms underlying perianal fistula formation are not well defined. Here, we dissected the tissue changes in the fistula area and addressed whether a dysregulation of extracellular matrix (ECM) homeostasis can support fistula formation.

METHODS: Surgical specimens from perianal fistula tissue and the surrounding region of fistulizing CD were analyzed histologically and by RNA sequencing. Genes significantly modulated were validated by real-time polymerase chain reaction,

Western blot, and immunofluorescence assays. The effect of the protein product of TNF-stimulated gene-6 (TSG-6) on cell morphology, phenotype, and ECM organization was investigated with endogenous lentivirus-induced overexpression of TSG-6 in Caco-2 cells and with exogenous addition of recombinant human TSG-6 protein to primary fibroblasts from region surrounding fistula. Proliferative and migratory assays were performed.

RESULTS: A markedly different organization of ECM was found across fistula and surrounding fistula regions with an increased expression of integrins and matrix metalloproteinases and hyaluronan (HA) staining in the fistula, associated with increased newly synthesized collagen fibers and mechanosensitive proteins. Among dysregulated genes associated with ECM, *TNFAI6* (gene encoding for TSG-6) was as significantly upregulated in the fistula compared with area surrounding fistula, where it promoted the pathological formation of complexes between heavy chains from inter-alpha-inhibitor and HA responsible for the formation of a crosslinked ECM. There was a positive correlation between TNFAI6 expression and expression of mechanosensitive genes in fistula tissue. The overexpression of TSG-6 in Caco-2 cells promoted migration, epithelial–mesenchymal transition, transcription factor *SNAI1*, and HA synthase (*HAs*) levels, while in fibroblasts, isolated from the area surrounding the fistula, it promoted an activated phenotype. Moreover, the enrichment of an HA scaffold with recombinant human TSG-6 protein promoted collagen release and increase of *SNAI1*, *ITGA4*, *ITGA42B*, and *PTK2B* genes, the latter being involved in the transduction of responses to mechanical stimuli.

CONCLUSIONS: By mediating changes in the ECM organization, TSG-6 triggers the epithelial–mesenchymal transition transcription factor *SNAI1* through the activation of mechanosensitive proteins. These data point to regulators of ECM as new potential targets for the treatment of CD perianal fistula. *(Cell Mol Gastroenterol Hepatol 2023;15:741–764; https://doi.org/10.1016/j.jcmgh.2022.12.006)*

Keywords: Perianal Fistula; Crohn's Disease; TSG-6; Extracellular Matrix; EMT.

See editorial on page 801.

Crohn's disease (CD) is a chronic bowel-relapsing inflammatory disorder[1] caused by transmural inflammation, that can affect any part of the gastrointestinal tract. CD phenotype can be variable according to risk of progression and depending on disease location behavior.[2] Perianal fistulae represent one of the most disabling manifestations of CD and is often associated with rectal disease involvement.[3] Moreover, fistula development represents a risk factor for more aggressive disease progression.[4] CD patients with perianal fistulae experience symptoms (eg, pain and fecal incontinence) that strongly impact on quality of life, with the risk of proctectomy and permanent ostomy in the most severe cases.[5] Current therapeutic options for CD perianal fistulae are limited and include antibiotics, immunomodulators, biologic agents, and mesenchymal stem cells,[6] in combination with surgical management. Nevertheless, the surgical removal remains the mainstay of fistula treatment, although it does not provide long-lasting results.[7] The etiopathogenesis of perianal fistula in CD is still unknown. The affected mucosa is destroyed and ulcerated and replaced by degranulation tissue. It appears infiltrated by inflammatory cells and myofibroblasts that, in the attempt to repair the damaged tissue, deposit collagen and other components of the extracellular matrix (ECM), with consequent tissue remodeling characterized by a high stiffness. Although some fistulae are not clearly associated with inflammatory processes, fistula development appears to be the result of the progression of inflammation through the mucosal wall, leading to the formation of unusual tunnel-like structures.[8] Fistula formation in CD is likely due to the epithelial–mesenchymal transition (EMT) of intestinal fibroblasts impairing the ability of these cells to repair mucosal membrane damage.[9,10] Specifically, by undergoing EMT, intestinal epithelial cells gain invasive and migratory properties and lose their cell polarity and cell-cell contacts, thus acquiring features of myofibroblasts.[11–16] However, the molecular mechanisms triggering EMT still remain to be investigated. An impaired expression of matrix metalloproteinases (MMPs) and tissue inhibitors of metalloproteinases was observed in CD fistulae,[17] supporting a dysregulated attempt of myofibroblasts to repair the damaged tissue that culminates in ECM remodeling. Of note, ECM, which is highly hydrated and composed of proteins and polysaccharides, in particular the glycosaminoglycan hyaluronan (HA), not only provides essential physical scaffolding for the cellular constituents, but also initiates crucial biochemical cues that are necessary for tissue morphogenesis, differentiation, and homeostasis.[18] In fact, HA associates with proteoglycan molecules that bind growth factors and also interacts directly with cell surface receptors to elicit downstream intracellular signal transduction and participates in the regulation of gene transcription.[19] The

***Authors share co-first authorship.**

Abbreviations used in this paper: **ActA, activin A; bFGF, basic fibroblast growth factor; BM, basement membrane; CCD, charge-coupled device; CD, Crohn's disease; cDNA, complementary DNA; DMEM, Dulbecco's modified Eagle medium; ECM, extracellular matrix; EMT, epithelial–mesenchymal transition; EV, empty vector; FBS, fetal bovine serum; FCS, fetal calf serum; FF, fistula-derived fibroblast; FFPE, formalin-fixed paraffin embedded; HA, hyaluronan; HBSS, Hank's Balanced Salt Solution; HC, heavy chain; HD, healthy donor; IαI, inter-alpha-inhibitor; IBD, inflammatory bowel disease; IL, interleukin; iHO, intestinal organoid; iPSC, induced pluripotent stem cell; MMP, matrix metalloproteinase; mRNA, messenger RNA; MW, molecular weight; OE, overexpressing; PBS, phosphate-buffered saline; PFA, paraformaldehyde; PFF, perifistula-derived fibroblast; qRT-PCR, quantitative real-time polymerase chain reaction; rhTSG-6, recombinant human TSG-6 protein; RNA-seq, RNA sequencing; RT-PCR, real-time polymerase chain reaction; TBS-T, Tris-buffered saline with Tween 20; TGFβ, transforming growth factor β; TNF-α, tumor necrosis factor α; TSG-6, TNF-stimulated gene-6.**

Most current article

2352-345X
https://doi.org/10.1016/j.jcmgh.2022.12.006

control of HA synthesis is, therefore, critical in ECM and cell biology. Alterations in the biochemical structure of the ECM also drive changes in tissue stiffness, which in turn could support the EMT process by creating a positive feedback loop.[20] Nevertheless, whether and how ECM disorganization contributes to EMT processes in fistula formation has not been investigated.

Here, we show, via a comparative transcriptome analysis between fistula tissue and its surrounding healthy region (named hereafter perifistula) in perianal fistulizing CD, that there is a different composition and architecture of the ECM between the 2 regions, with an increased expression of matrix-associated regulators and mechanosensitive proteins in the fistula tract compared with the perifistula. To address the functional role of ECM changes in the fistula, we focused on the increase of the protein product of TNF-stimulated gene-6 (TSG-6), an ∼35-kDa protein that, in addition to exerting strong anti-inflammatory and tissue-protective properties,[21] serves also as a regulator of ECM organization/function and is implicated in the transduction of extracellular signaling into cells.[22] By forming covalent complexes between HA and the heavy chains (HCs) of inter-alpha-inhibitor (IαI) (termed HC•HA), TSG-6 participates in altering the structural organization of HA in the ECM of fistula. Our in vitro functional assays indicated that the epithelial overexpression of TSG-6 promotes HC•TSG-6 complex production, an intermediate in the formation of HC•HA and promotes the induction of the EMT transcription factor *SNAI1* through the activation of mechanosensitive proteins. Therefore, we propose that the mechanochemical signaling of the ECM in the fistula can promote the perpetuation of the disease by supporting the EMT process, thus unveiling new pathophysiological processes of fistula formation and paving the way for new potential therapeutic approaches.

Results

ECM Organization Discriminates Fistula From Perifistula Tissue

In order to investigate the overall tissue changes in perianal fistula, we performed transcriptome analysis by RNA sequencing (RNA-seq) of resected tissue collected from both fistula and nonlesioned tissue (perifistula) of CD patients (n = 8 for both groups). To ensure correct tissue identification and harvesting, fistula and perifistula tissues were first examined histologically. As shown in Figure 1*A*, the fistula area (outlined by white dotted lines) was surrounded by granulation tissue and characterized by the presence of inflammatory cell infiltration as also indicated by the upregulation of inflammatory cytokines (interleukin [IL]-6, tumor necrosis factor α, and transforming growth factor β1 [TGFβ1]) compared with perifistula area (Figure 1*B*). Both analyses revealed clear differences in the morphology and inflammatory status between the 2 analyzed areas. Accordingly, t-distributed stochastic neighbor embedding multidimensional scaling of transcriptomic data revealed extensive clustering of fistula and perifistula areas within the lower left or upper right corners of sample dispersion, respectively (Figure 1*C*). Out of the 8172 genes that were significantly ($P < .5$) differentially expressed, 3785 genes were upregulated and 4387 genes were downregulated in fistula compared with the perifistula as illustrated in the MA plot (Figure 1*D*) and by a hierarchically clustered heatmap (Figure 1*E*). Gene set enrichment analysis on the significantly differentially expressed genes showed involvement in signaling pathways associated with multiple biological processes (ie, based on the Gene Ontology categories being modulated with statistical significance) (Figure 1*F*). Not surprisingly, gene sets related to the signatures of EMT, immune response, and ECM were significantly enriched in the fistula compared with the perifistula tissue, consistent with the histological features. In addition, in the fistula we noticed an enhancement of genes associated with HA biosynthetic process, ECM assembly, and negative regulators of signal transduction, suggesting differences in ECM organization and cell-matrix interaction between the 2 areas. To further explore this, we looked at the (significant) differential genes within ECM/adhesion-related Gene Ontology categories. The hierarchically clustered heatmap (Figure 2*A*) in the fistula area revealed a significant decrease of integrins; adhesion molecules; a significant modulation of the HA pathway characterized by an increase of HA synthase enzymes, *HAS1* and *HAS2*; and a decrease of its receptors and binding proteins (ie, *CD44* and HA and proteoglycan link protein 1 [*HAPLIN1*]). The increase of *HAS1* and *HAS2* and the decrease of *CD44* were further validated on a larger number of patients (n = 20 by real-time polymerase chain reaction [RT-PCR] analysis) (Figure 2*B*).

Consistent with the modulation of collagen gene expression, Sirius red staining showed a visible accumulation of collagen deposition in the fistula region, as confirmed by the semiquantitative quantification in Figure 2*C*. Notably, the analysis of collagen using polarizing microscopy, which informs on the maturation state of the collagen fibers,[23] revealed an accumulation in the fistula of newly synthesized collagen fibers with green/yellow birefringence ($P < .032$) compared with perifistula region, which was enriched with thick collagen fibers with red birefringence ($P < .0001$) typical of long-term collagen fibers (Figure 2*D*). Hierarchical clustering of collagen genes, differentially expressed between fistula and perifistula tracts ($P < .05$), showed an upregulation of multiple types of collagens in the fistula compared with the perifistula; this included fibrillar collagens such as collagen III (*COL3A1*), collagen V (*COL5A1* and *COL5A2*), and collagen XXIV (*COL24A1*); the fibrillar-associated (with interrupted triple helices, known as FACIT) collagens IX (*COL9A1*), XII (*COL12A1*), XIX (*COL19A1*), and XXII (*COL22A1*); the basement membrane (BM) collagen IV (*COL4A1* and *COL4A2*); and the BM-associated collagen VI (*COL6A1*, *COL6A2*, and *COL6A3*) (Figure 2*E*). Conversely, collagen XVII (*COL17A1*), a transmembrane collagen mediating the attachment of keratinocytes to the underlying BM, was markedly downregulated (Figure 2*E*) along with *COL4A5* and *COL4A6*, which form a type of collagen IV specifically associated with the intestinal epithelial BM. ECM remodeling is finely regulated by a dynamic equilibrium of its production and degradation by the

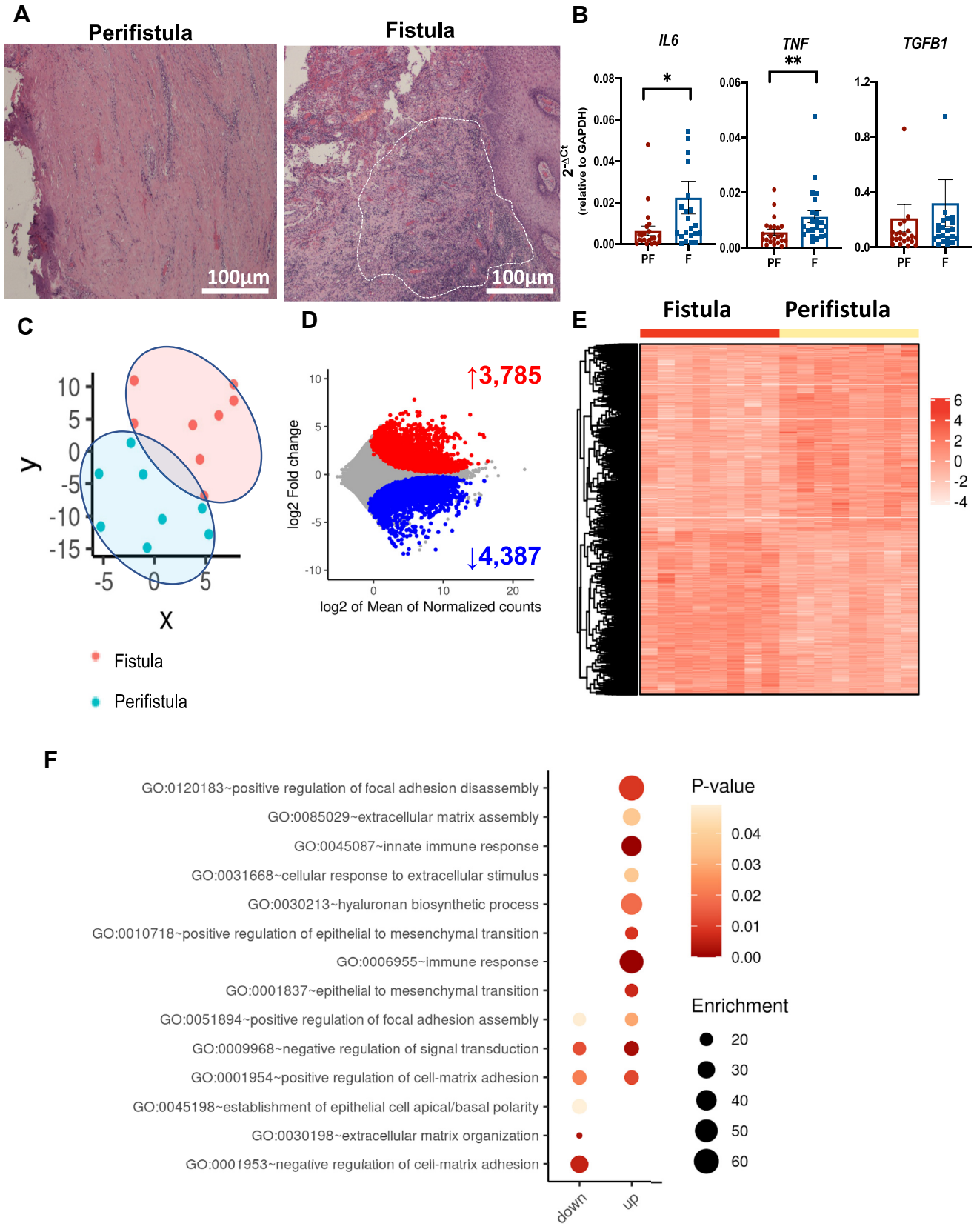
A
Perifistula
Fistula
100µm
100µm
B
IL6
TNF
TGFB1
*
**
2^-ΔCt (relative to GAPDH)
PF
F
C
y
X
Fistula
Perifistula
D
↑3,785
↓4,387
log2 Fold change
log2 of Mean of Normalized counts
E
Fistula
Perifistula
F
GO:0120183~positive regulation of focal adhesion disassembly
GO:0085029~extracellular matrix assembly
GO:0045087~innate immune response
GO:0031668~cellular response to extracellular stimulus
GO:0030213~hyaluronan biosynthetic process
GO:0010718~positive regulation of epithelial to mesenchymal transition
GO:0006955~immune response
GO:0001837~epithelial to mesenchymal transition
GO:0051894~positive regulation of focal adhesion assembly
GO:0009968~negative regulation of signal transduction
GO:0001954~positive regulation of cell-matrix adhesion
GO:0045198~establishment of epithelial cell apical/basal polarity
GO:0030198~extracellular matrix organization
GO:0001953~negative regulation of cell-matrix adhesion
down
up
P-value
Enrichment

activity of MMPs. In this regard, RNA-seq showed that *MMP9*, *MMP13*, *MMP19*, *MMP25*, and *MMP26* were significantly upregulated in the fistula region, indicative of increased breakdown of extracellular collagens during tissue degeneration (Figure 2*F* and *G*). Overall, changes to the collagen network and increased synthesis of HA are likely to impact the tensile strength and swelling properties of the tissue, perhaps explaining the stiffening of the fistula region observed clinically.

TSG-6 Expression Increases in the Fistula Tract

To gain better insight into ECM dysfunction in CD fistula, we further analyzed the core matrisome genes as described by Naba et al.[24] Interestingly, within the list of significantly affected genes, as well as collagen subunits, proteoglycans, and glycoproteins involved in the architecture of ECM, we detected that *TNFAIP6*, encoding for the TSG-6 protein, a regulator of ECM organization/function and cell signaling, was significantly upregulated in the fistula area (Figure 3*A*). Its upregulation was confirmed on a larger cohort of perianal tissue sample (n = 20) at the RNA level by quantitative RT-PCR (qRT-PCR) (Figure 3*B*) and at the protein level by Western blot when compared with healthy region ($P < .05$) (Figure 3*C*). Although TSG-6 exerts anti-inflammatory and tissue protective functions,21 it also catalyzes a covalent modification of HA by facilitating the transfer of HC via a transesterification reaction. TSG-6 induced HC•HA complex formation were observed in several pathological conditions including inflammatory bowel disease (IBD).[21,25–28] To explore if TSG-6 participates in the HA modification, first we assessed colocalization of both TSG-6 and HA (using biotin-HABP) using immunofluorescence on tissue. The immunostaining revealed that TSG-6 and HA were coexpressed by both epithelium and stromal compartments in the fistula (Figure 3*D*, right panel). In the perifistula, conversely, the immunoreactivity for TSG-6 was not detected in the epithelium, and scarcely in the stroma, whereas HA was everywhere abundant (Figure 3*D*, left panel). Then, we evaluated the formation of HC•HA, by performing a co-immunostaining of HA with an anti-IαI antibody that recognizes HCs (HC1, HC2, and HC3) and bikunin (Figure 4). In the perifistula area, IαI staining was completely negative (Figure 4, left panel), while in the fistula region it was strongly positive and colocalized with HABP (Figure 4, middle panel). No difference was found in the staining of HA, TSG-6, and IαI between the perifistula region and healthy tissue collected from non-IBD patients (Figure 4, right panel), indicating no precommitted alterations of ECM organization in the area surrounding the fistula.

Overall, these results indicate that the upregulation of TSG-6 in the fistula tract correlated with the accumulation of HA and likely participates in the formation of pathological HC•HA complexes.

TSG-6 Drives EMT in Caco-2 Cells

A previous study demonstrated that a transient upregulation of TSG-6 in renal tubular epithelial cells promotes the EMT process by modulating HA assembly.[29] In order to investigate whether the marked expression of TSG-6 in epithelial cells plays a role in the EMT process associated with fistula formation, we overexpressed TSG-6 by lentiviral transduction in epithelial Caco-2 cells, which do not express TSG-6 under normal conditions (Figure 5*A*). After 72 hours of transduction, cells were collected and tested for EMT-related genes, proliferation, and migration.

TSG-6 expression was validated by quantitative RT-PCR, which showed a 60-fold-increase of expression in the TSG-6-overexpressing (OE) cells compared with cells that had integrated the expression cassette not containing the TSG-6 complementary DNA (cDNA) sequence (empty vector [EV], $P < .001$) (Figure 5*A*). The increased levels of TSG-6 were detected at an apparent molecular weight (MW) of ∼40 kDa (close to that expected for the free protein) by Western blot analysis on cell lysates (Figure 5*B*). To test whether TSG-6 overexpression promoted HA•HC formation in the extracellular compartment, we analyzed the TSG-6 species present in the cell culture supernatants. While the levels of free TSG-6 were low (but detectable) in TSG-6 OE cells, there was an intense band at an apparent MW of ∼150 kDa that was greatly reduced in intensity by NaOH treatment but not by chondroitinase ABC lyase (Figure 5*C*). This is consistent with this ∼150-kDa species corresponding to a covalent HC•TSG-6 complex, in which the HC and TSG-6 proteins are linked via an ester bond, as has been described previously.21,37 Importantly, HC•TSG-6 is a well-established intermediate in HC•HA formation.

We next assessed the expression of 2 EMT markers, E-cadherin (*CDH1*), an epithelial marker, significantly decreased, and Snail (*SNAI1*), a mesenchymal marker significantly enriched in the fistula tract as shown by RNA-seq (Figure 5*D*, left panel) and then validated on a larger cohort of perianal tissue samples by qRT-PCR (Figure 5D, right panel). Accordingly, *SNAI1* expression increased in TSG-6 OE cells compared with EV cells ($P < .05$), while no difference in *CDH1* expression was found between 2 cell populations (Figure 5*E*). Moreover, the overexpression of TSG-6 significantly attenuated the proliferative capacity of Caco-2 cells 48 hours after plating (Figure 5*F*) and enhanced

Figure 1. (*See previous page*). CD-associated fistula displays a distinct transcriptome profile compared with perifistula. (*A*) Histological representative images underline the differences from the same patient between perifistula and fistula (outlined by white dotted lines) regions by hematoxylin and eosin. Scale bar = 100 μm. (*B*) Relative transcript levels of *IL-6*, *tumor necrosis factor* α, and *TGF*β*1*. The results were normalized to *GAPDH* and data presented as mean ± SEM.*$P < .05$, **$P < .01$ by Mann-Whitney test. n = 22 patients. (*C*) t-Distributed stochastic neighbor embedding plot visualizing cluster assignments of samples, in which samples are projected in t-distributed stochastic neighbor embedding space. (*D*) Volcano plot representing upregulated and downregulated genes in fistula vs perifistula samples. (*E*) Heatmap of differentially expressed genes in fistula and perifistula samples. (*F*) Gene Ontology (GO) plot–enriched pathways in fistula vs perifistula biopsies with respective *P* values and enrichment score (n = 8, analysis between perifistula and fistula regions from the same patient).

the migratory ability of Caco-2 cells at 24 and 48 hours ($P = .0003$ and $P = .0081$, respectively) (Figure 5*H* and *G*). To determine if the biological response of Caco-2 cells to TSG-6 was dose-responsive, we conducted the migration assay in the presence of a low (5 ng) and high (10 ng) concentration of recombinant human TSG-6 protein (rhTSG-6). Both

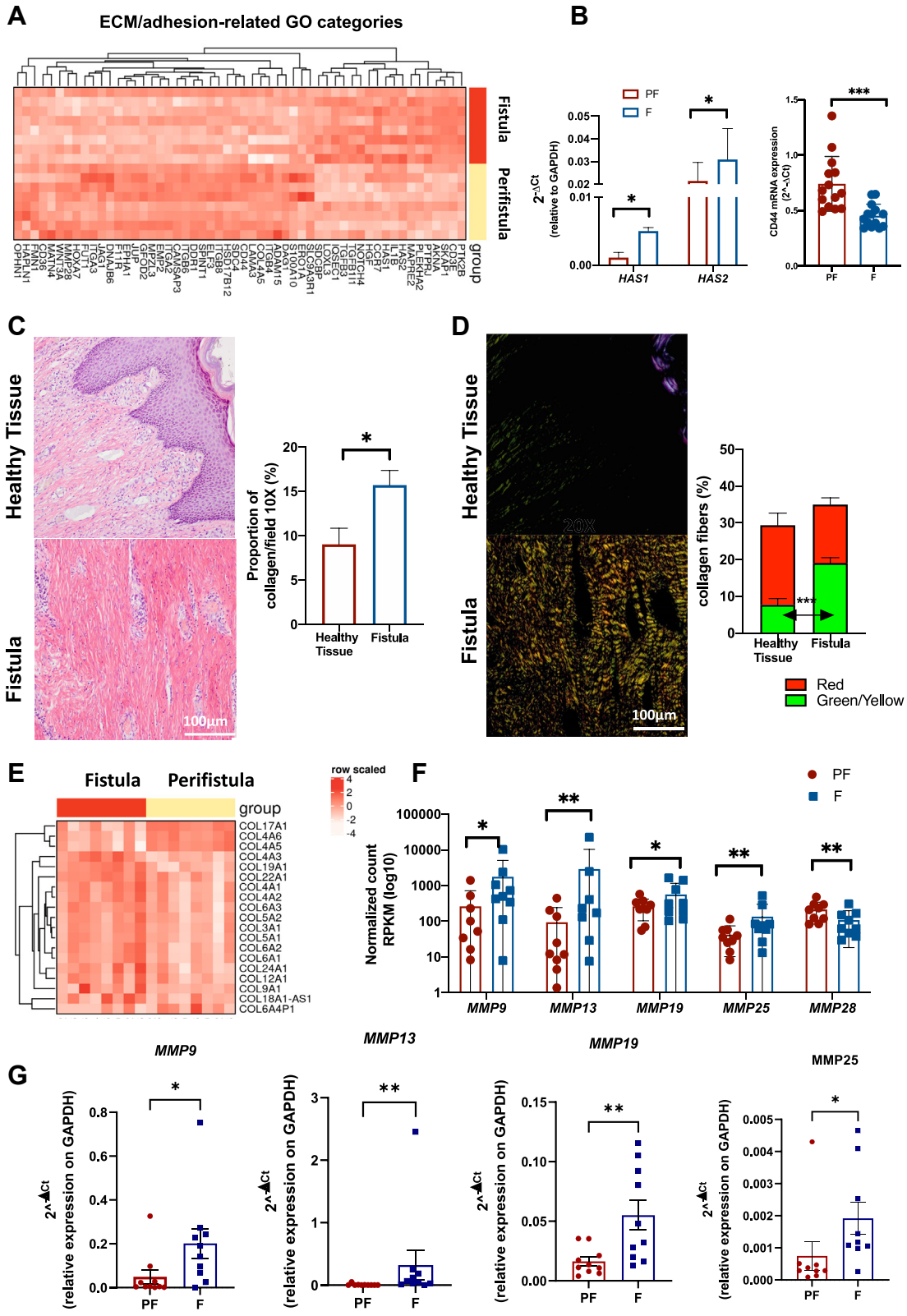

concentrations significantly promoted cell migration 24 and 48 hours postscratch (Figure 6). Collectively, these data suggested that the overexpression of TSG-6 promotes the formation of HC•TSG-6 complexes in the extracellular compartment and participates in cellular processes typically observed in cells undergoing EMT by promoting epithelial cell transdifferentiation and migration but reducing proliferation.

TSG-6 Is Required in the EMT

To further corroborate TSG-6 as a mesenchymal gene associated to the mesenchymal transition process, we analyzed its expression during the reprogramming process of mesenchymal–epithelial transition (MET), when mesenchymal genes are repressed through the generation of human induced pluripotent stem cell (iPSC)–derived intestinal organoids (iHOs) from adult fibroblasts. To this end, commercial dermal fibroblasts isolated from a skin of an female healthy donor (HD) were reprogrammed by expression of the transcription factors of OCT4, SOX2, KLF4, and c-MYC.[30,31] iPSC-like colonies were individually picked 4 weeks later, expanded, and characterized. The clones showed an iPSC-like colony morphology, a normal 46,XX karyotype, and stemness markers and were able to differentiate in vitro, as shown by positivity to all 3 germ-layer markers (Figure 7*A*–*D*). HD-iPSCs were forced to differentiate into iHOs,[32] and iPSC-derived iHOs were analyzed after 30 days in Matrigel (BD Biosciences, San Jose, CA) (Figure 8*A*). They showed a crypt-villus architecture of the intestine (Figure 8*B*) and the presence of typical cell types of the intestinal tissue, including cytokeratin 19, epithelial cellular adhesion molecule, E-cadherin, and structural protein of tight junctions zona occludens-1 indicating the presence of apical tight junctions facing the lumen of the organoid (Figure 8*C*–*E*). They also showed ubiquitous expression of enterocyte marker villin, with specific subset of cells expressing mucin 2 and chromogranin A, markers associated with the goblet and enteroendocrine cells, respectively, confirming the correct differentiation of iPSCs into iHOs (Figure 8*F*–*H*). According with Caco-2 results, TSG-6 expression was scarce in iHOs (Figure 8*I*–J). TSG-6 messenger RNA (mRNA) expression level was highly expressed in correlation with the levels of the transcriptional factor *SNAI1* on fibroblasts, and both genes were drastically reduced as well as vimentin, an mesenchymal marker, when iHOs were well established (Figure 8*L*), as demonstrated by a concomitant upregulation of key epithelial genes such as *CDH1* and *LGR5*, recognized as markers of differentiated epithelial cells and adult stem cells, respectively. Overall, these data pointed out TSG-6 as a gene required/involved in the conversion of epithelial cells into mesenchymal cells independently of tissue of origin.

TSG-6 Overexpression Impacts Fibroblast Phenotype

Upon fistula formation, the transdifferentiation of epithelial cells into mesenchymal cells compensates for the pathological inhibition of the migration of the tissue-resident fibroblasts.[9,10] During this process, transdifferentiated cells gain migratory properties and a high capacity to synthesize ECM components. Interestingly, resident fistula-derived fibroblasts (FFs) expressed higher amounts of TSG-6 compared with those isolated from perifistula (perifistula-derived fibroblasts [PFFs]) ($P < .01$) together with an increase in *SNAI1* (a transcriptional factor that controls fibroblast migration) expression (Figure 9*A*). To determine if the overexpression of TSG-6 induced *SNAI1* upregulation, we overexpressed TSG-6 in PFF and quantified its mRNA expression levels (Figure 9*B*). *SNAI1* mRNA levels increased in PFF TSG-6 OE cells compared with EV control cells (Figure 9*B*). In addition, TSG-6 OE PFF cells displayed elevated expression of *HAS2*, and although not significant, expression of *ACTA2* (commonly referred to as alpha-smooth muscle actin), a marker of fibroblast activation (Figure 9*C*). These molecular changes were also accompanied by the acquisition of different cellular morphology. While PFF EV control cells appeared spindle shaped with cytoplasmic bipolar projections, TSG-6 OE PFF cells showed enlarged cytoplasm with plump nuclei characterized by finely dispersed chromatin and conspicuous nucleoli (Figure 9*D* [left panel] and *E*) indicative of a transcriptionally active status. Interestingly, the overexpression of TSG-6 in the PFFs drove morphological changes that resembled those of the FFs, as also evidenced by F-actin immunolabeling (Figure 9*D*, right panel).

Changes in ECM Organization Drive the Activation of Mechanosensors

Changes of ECM structure can translate into the activation of intracellular responses via collagen fibers and focal adhesions through a process defined as mechanotransduction, which in turn triggers the activation of several nuclear transcription factors.[33] Our RNA-seq highlighted a significant upregulation of several genes that mediate mechanotransduction-mediated

Figure 2. (***See previous page***). **ECM reorganization in CD-associated fistulae.** (*A*) Heatmap highlighting the differences in genes related to ECM in fistula vs perifistula biopsies (n = 8, analysis between perifistula and fistula regions from the same patient). (*B*) *HAS1*, *HAS2*, and *CD44* gene expression by qRT-PCR in fistula vs perifistula tract from the same patient by qRT-PCR (n = 14). (C) Sirius red staining showing collagen deposition in fistula tract from pooled samples of CD patients (n = 15) and in healthy tissue (HT) of anus from non-IBD patients (n = 7). Scale bar = 100 μm. In the right panel, the percentage of total collagen deposition is shown. (*D*) Representatives images of the polarized light microscopy showing the different type of collagen fibers (green-yellow and red) between fistula (n = 15) and HT (n = 7) areas and their enrichment in percentage in the right panel. (*E*) Heatmap representing the expression of collagen genes in fistula and perifistula areas from the same patient (n = 8). (*F*) Relative transcript levels by RNA-seq analysis (n = 8 patients) and (*G*) mRNA levels by qRT-PCR of *MMP9*, *MMP13*, *MMP19*, *MMP25*, and *MMP28* in fistula and perifistula areas (n = 10 patients). Biological triplicates for each group. Data are presented as mean ± SEM. **P* < .05, ***P* < .01, ****P* < .001, and **** *P* < .0001 by Mann-Whitney test (*B–D*, *G*).

signaling pathways including integrins and protein tyrosine kinases in the fistula compared with the perifistula tissue (Figure 10*A*). The paired comparison analysis of RNA-seq data between perifistula and fistula areas from the same patient revealed *ITGA4*, *ITGA2B*, *ITGB7*, *FUT8*, *NEDD9*, and *PTK2B* highly upregulated in the fistula (Figure 10*B*). The correlation heatmap depicting the measure of dependence between multiple variables, showed a positive correlation of TSG-6 (*TNFAIP6*) with *ITGA4* and *ITGA2B*, genes encoding for integrins, and protein tyrosine kinase 2B gene (*PTK2B*) ($P < .05$) (Figure 10*C*).

To explore if HA accumulation and overexpression of TSG-6 can impact ECM organization promoting the activation of mechanosensors in fibroblasts, we plated PFFs on top of a HA-based HyStem hydrogel scaffold, in the absence (nonsupplemented) and presence (supplemented) of rhTSG-6 (Figure 11*A*) at a concentration that is known to crosslink and stiffen HA.[22,34] After 24 hours at 37°C, the cell culture supernatants were analyzed for collagen content and the cells for *ITGA4*, *ITGA2B*, *PTK2B*, and *SNAI1* expression. Interestingly, when cultured on the scaffold, PFFs significantly increased the collagen release ($P < .05$), and this was elevated further in the presence of rhTSG-6 ($P < .001$) (Figure 11*B*). Because IL-6 is a potent inducer of collagen production in fibroblasts,[35] we checked its levels in the cell culture supernatants. Accordingly, IL-6 levels increased in correlation with collagen amounts in plated PFF cells on both scaffolds (Figure 11*C*). Interestingly, seeding cells on the nonsupplemented scaffold promoted the transcription of *SNAI1*, *ITGA2B*, *ITGA4*, and *PTK2B* compared with cells plated without scaffold (no scaffold) (Figure 11*D*–*G*). However, the enrichment of the scaffold with rhTSG-6 significantly augmented the expression of all these genes compared with the nonsupplemented scaffold or on the plate without scaffold ($P < .005$), to a level similar to the FFs (Figure 11*D*–*G*). Similar results were obtained with non-IBD healthy fibroblasts (data not shown), indicating that the remodeling of ECM contributes to the activation of mechanosensors that in turn activate nuclear transcription factors.

Discussion

In this study, we provided evidence that an altered organization of the ECM in the perianal fistula of CD, exhibiting high collagen deposition, increased HA synthesis, and the presence of HA-binding proteoglycans/proteins, may participate in sustaining the pathological epithelial-to-mesenchymal transition events underlying perianal fistula formation. A dysregulated EMT is associated with a variety of pathologies including fibrotic diseases,[36] cancer,[37] and fistula,[15] in which it intervenes in replacing the impaired activity of resident fibroblasts to repair intestinal damage.[9,10] Several studies reported the increased levels of IL-13 and TGFβ as the critical cues in triggering EMT in the perianal fistula of CD patients, thus supporting the chronic inflammatory processes as important in promoting fistula formation. The perianal fistula area, in fact, is infiltrated by inflammatory cells including T cells, B cells, and macrophages that sustain these EMT events by releasing a plethora of proinflammatory mediators.[8] Accordingly, our data showed evidence of an increased immune response in the fistula area and upregulation of genes associated with the EMT processes, including *IL-13* (Figure 12). To date, standard medical management has been traditionally based on the use of antibiotics and immunomodulators, which includes the use of biologic agents[6] targeting the massive immune infiltration. However, incomplete (or a lack of) response to medication is frequent in these patients, for whom surgical removal of the fistula becomes necessary with disabling consequences.[6] This suggests, therefore, that dampening inflammation is not enough to restore mucosal homeostasis and to arrest the EMT processes in perianal fistulizing CD patients.

However, what other factors contribute to these pathological processes remain unknown. Here, we showed for the first time that changes in ECM organization likely promote mechanical signals supporting EMT. ECM remodeling is essential in mucosal repair consequent to an inflammatory response and granulation tissue formation, and in maintaining a correct re-epithelialization of the tissue; for example, the polarization along the apical-basal axis of the epithelium is mediated by the attachment to the basement membranes. Several collagens such as COL17A1, COL4A5, and COL4A6 that stabilize the attachment of intestinal epithelial cells to BM were markedly downregulated in the fistula area. The loss of cell-BM contacts is a first hallmark of EMT.[37] Therefore, EMT is highly influenced and controlled by the surrounding ECM. We found deposits of newly synthetized fibril-forming interstitial collagens (mainly type III) and BM collagens (type IV) to be increased in the fistula; these collagens consist of multiple isoforms that support cell adhesion and maintain normal tissue architecture and function.[38] The expression of *MMP9, MMP13, MMP19, MMP25,* and *MMP26* critical to regulate ECM degradation are increased. Moreover, the fistula area is enriched in the polysaccharide HA that is likely associated with the formation of a pathogenic matrix. HA is an essential structural component of the ECM that, along with bound chondroitin sulfate proteoglycans and link proteins (such as HAPLN1), regulates tissue turgor and thus contributes to the biomechanical properties of tissues. HA biosynthesis is dysregulated in inflammation and in response to tissue damage, and invasion by tumor cells or pathogens[19,39]; it is upregulated in many pathological conditions, including IBD,[40,41] and accumulates in the lungs of patients with influenza A and SARS-CoV-2 infection,[42,43] which in the latter is driven by IL-13. Here, 2 enzymes that mediate HA synthesis, *HAS1* and *HAS2*, were found to be increased in perianal fistula of CD patients, whereas *HAPLN1* was decreased, indicative of ECM remodeling. TSG-6, which is often induced in inflammation,[21,44,45] was also upregulated in the fistula area. TSG-6 is a multifunctional, ~35-kDa, secreted protein that interacts with a wide range of ligands and has been found to have anti-inflammatory properties in many different contexts,[21] including in models of colitis,[46,47] and also has tissue protective effects, for example, promoting wound healing.[21,48–51] In a previous study,[52] we demonstrated that TSG-6 plays a crucial role in the mucosal healing processes mediated by HA. One of TSG-6's functions is to act as an

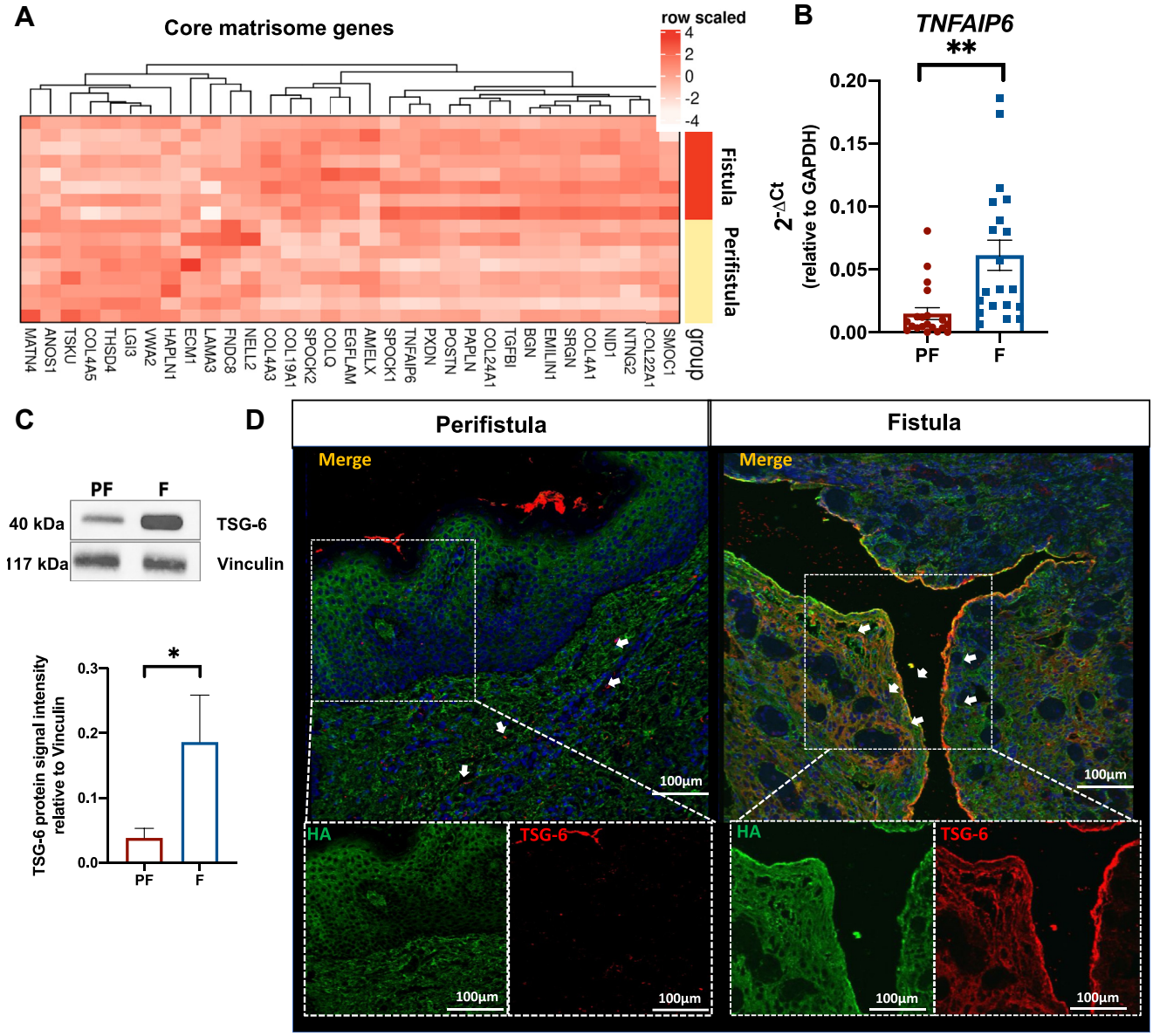

Figure 3. TSG-6 is upregulated in fistula compared with perifistula regions and mediates pathological HC•HA complex formation. (*A*) Heatmap representing the expression of matrisome core genes (n = 8 patients). (*B*) Relative transcript levels of *TNFAIP6* in fistula and perifistula areas from the same patients (n = 20). (*C*) Representative Western blot analysis of TSG-6 and vinculin as control, in whole cell lysate from fistula and perifistula areas. Below, TSG-6 protein signal intensity quantification relative to vinculin (n = 5 patients for each group). (*D*) Immunofluorescence staining of TSG-6 (red) and HA (green) in fistula area (left panel) and in fistula tract (right panel) from the same patient. DAPI = nuclei in blue. Scale bar = 100 μm. Data are presented as mean ± SEM. *$P < .05$, **$P < .01$ by Mann-Whitney test.

enzyme in the covalent transfer of HCs from IαI onto HA, where HC•TSG-6 complexes act as intermediates in this process.[21,53] The TSG-6–mediated production of HC•HA leads to the formation of a crosslinked, expanded, HA matrix that is essential for ovulation and fertilization,[21,54] and for gut asymmetry during development[55]; the crosslinking, and thus stabilization of the matrix, likely occurs through HC-HC interactions[56] and via binding of HCs to pentraxin-3.[57] Moreover, HC•HA complexes (containing pentraxin-3) are thought to be responsible for the potent anti-inflammatory, antifibrotic, and antiangiogenic properties of amniotic membrane.[26] The formation of HC•HA also occurs in tissues during inflammation (ie, at sites where TSG-6 is expressed and where IαI has ingressed from the blood circulation).[21] Whether the HC•HA complexes are protective or drive pathology is likely dependent on their compositions (ie, which HCs are covalently attached to HA and whether accessory molecules, such as pentraxin-3, are bound) and the context of their formation. For example, in lung conditions, such as cystic fibrosis,[58] airway hyperresponsiveness,[59] and influenza A infection,[43] HC•HA contributes to a pathogenic matrix, with increased numbers of associated immune cells.

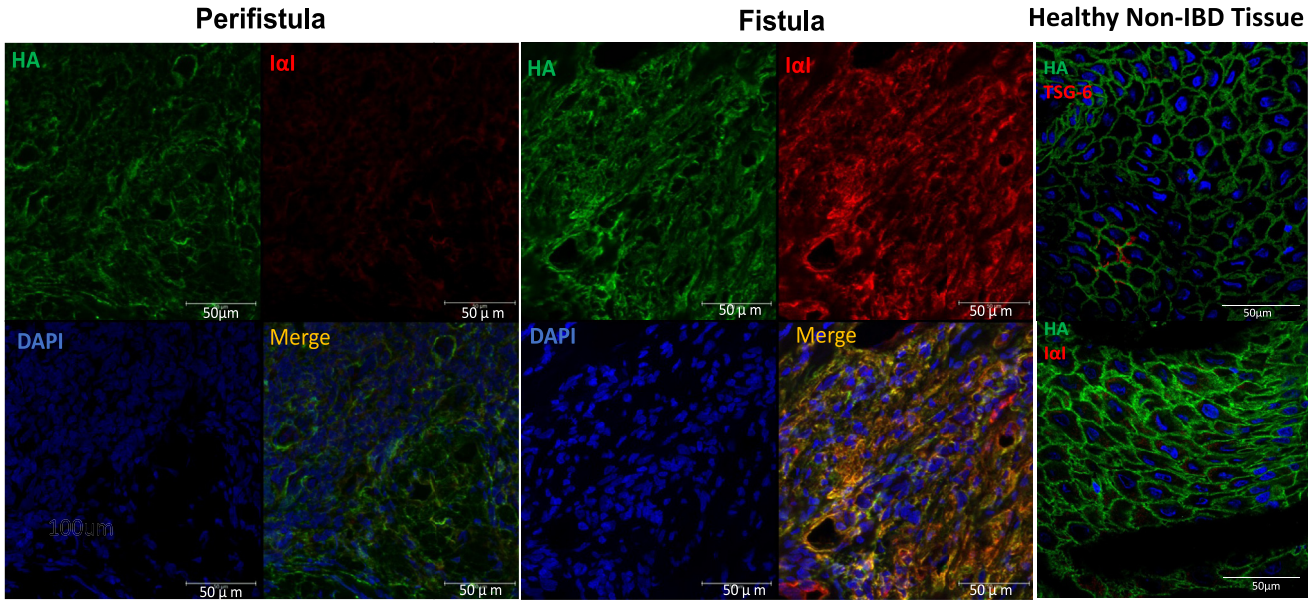

Figure 4. Immunostaining for HA and IαI expression in fistula and healthy anal tissue. Representative images of immunofluorescence staining of IαI or TSG-6 (red) and HA (green) in perifistula (left panel) and fistula (middle panel) regions from the same CD patient and in healthy anal tissue of non-IBD patients (right panel). DAPI = nuclei in blue. Scale bar = 50 μm.

The finding here that there is increased staining for HA, IαI, and TSG-6 in fistula strongly suggest that HC•HA complexes are being formed, such that crosslinking interactions have the potential to alter the mechanical properties of the tissue (eg, in conjunction with collagen deposition). Furthermore, TSG-6 in absence of IαI[60] has been found to have a dramatic effect on HA structure, collapsing and stiffening the HA network.[21,34] Thus, the relative amounts of TSG-6 and IαI could tune the mechanical properties of the HA matrix.

TSG-6–mediated crosslinking of HA has been found to enhance its interaction with CD44 on leukocytes[60,61] and may be responsible for some of TSG-6's anti-inflammatory effects[52,62,63] HC•HA has also been implicated in supporting immune cell adhesion, which in this case it is likely associated with pathology.[25,43,58,59] Thus, given the different activities for HA/TSG-6 and HC•HA complexes, it is difficult to interpret the decrease in expression of *CD44* in the fistula area seen in the present study.

Interestingly, TSG-6 overexpression in Caco-2 cells led to HC•TSG-6 complex formation in the culture supernatants. Although the experiments were performed in serum-free conditions without adding exogenous IαI, there was clearly sufficient IαI present to lead to the formation of HC•TSG-6, as this species was much more abundant than the free TSG-6 protein; in this regard, it is very difficult to remove IαI because it tightly adheres to the cell surface. Given that it is well established that HA is synthesized by epithelial cells, it seems likely that HC•HA complexes will be formed, in which these, for example, have been implicated in the TGFβ–mediated differentiation of fibroblasts to myofibroblasts.[64] In this regard, TSG-6 overexpression in Caco-2 cell significantly induced the expression of the EMT transcription factor Snail. Accordingly, TSG-6 OE cells exhibited high migratory capacities but reduced the proliferative capacity of Caco-2 cells, an effect also observed in human endothelial cells.[65] The overexpression of TSG-6 in the PFFs promoted their activation. Indeed, the cells displayed increased levels of *ACTA-2*, gene encoding for the α-smooth muscle actin marker of myofibroblast activation and of *SNAI1*, and morphological changes resembling those of FFs. The involvement of TSG-6 in inducing these alterations in the cellular morphology and cytoskeletal architecture is also supported by our previous work demonstrating that the enrichment of ECM with TSG-6 in mesenchymal stem cells promoted the reorganization and polymerization of the actin cytoskeleton.[22] The marked reduction of TSG-6 in the reverse process from mesenchymal to epithelial reprogramming observed on iPSC-derived iHOs further corroborated it as a mesenchymal gene involved in the transition process of the fibroblasts independently from tissue of origin. As discussed previously, it is reasonable to assume that the modification of HA by TSG-6 induces changes in the biomechanical properties of the ECM, which in turn propagates mechanotransduction via actin cytoskeleton modifications and activation of intracellular signaling pathways.[33,40] In support of this hypothesis, the enrichment of the HA scaffold with TSG-6 activated some integrins that serve as mechanosensitive proteins in PFFs.

Cell adhesion to the ECM is, indeed, regulated by integrins: transmembrane receptors that interact with matrix components (eg, fibronectin and vitronectin) via their extracellular domains and also interact with actin via their cytoplasmic. Several of these integrins, in particular, integrin alpha 4 (*ITGA4*) and integrin alpha 4 subunit 2b (*ITGA42B*) and the associated protein-tyrosine kinase 2-beta (*PTK2B*) that are all involved in activating pathways leading to actin cytoskeletal rearrangements and transcriptional

alterations,[66] were upregulated in the fistula area. Moreover, their expression was induced after the enrichment of ECM with HA and TSG-6 in a quantity demonstrated to make the HC•HA complex formation.[34] Nevertheless, HA alone was enough to stimulate collagen deposition, and the supplementation with rhTSG-6 further enhanced this finding.

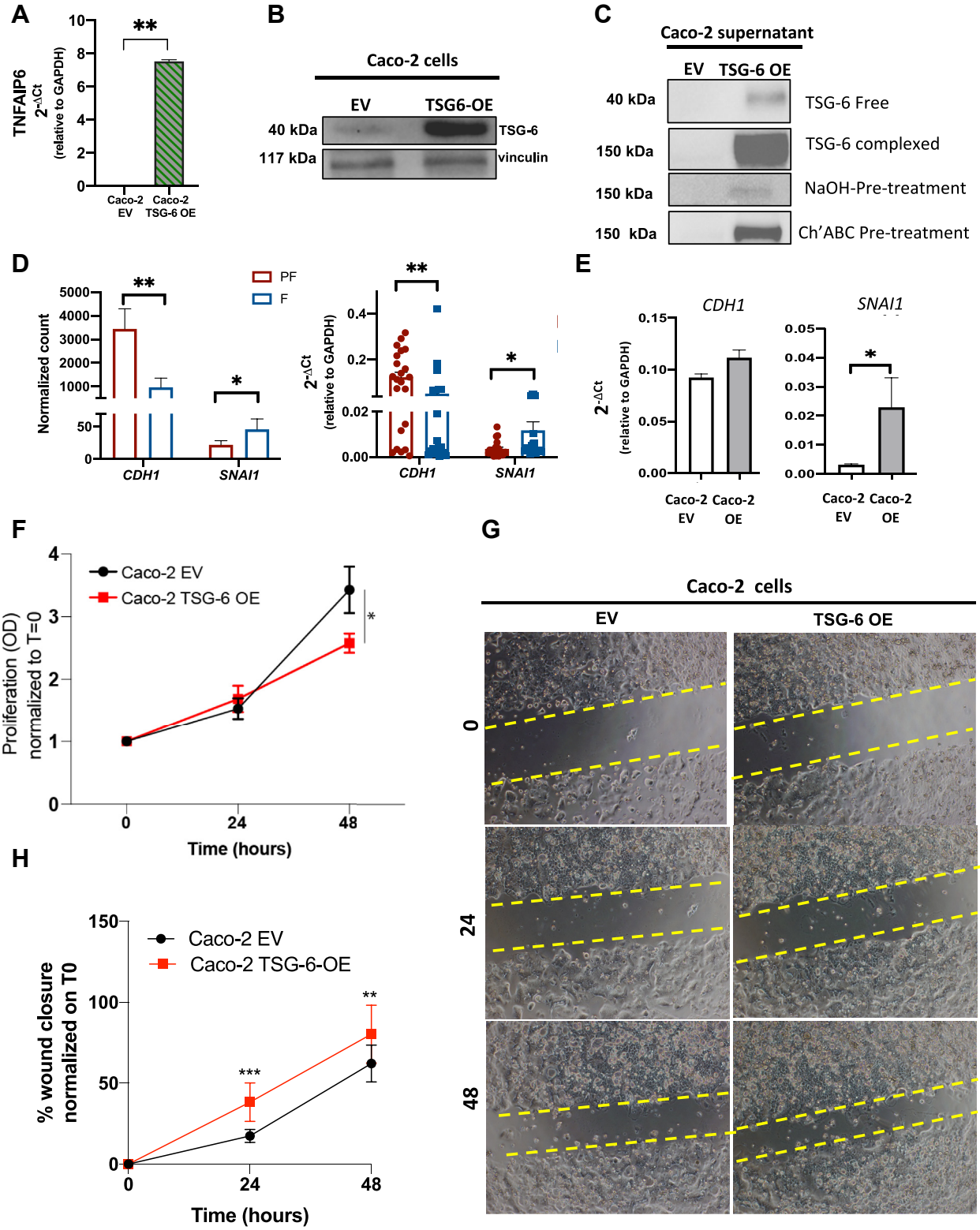

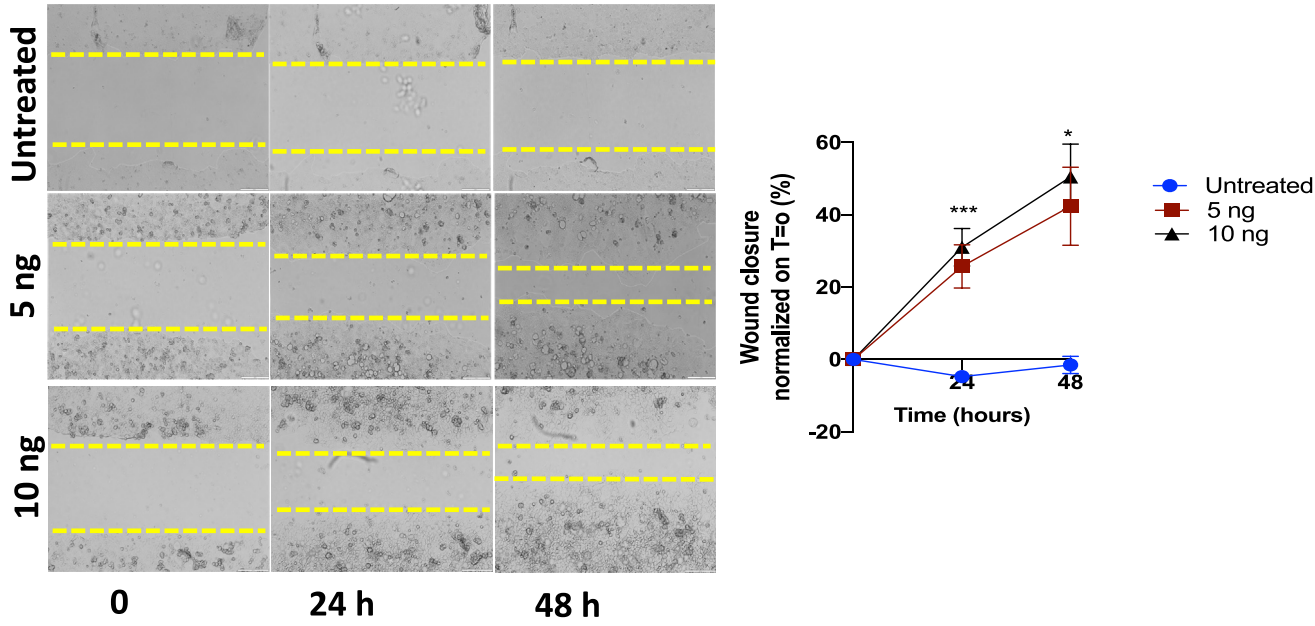

Figure 6. TSG-6 induces migration in Caco-2 cells in a dose-dependent manner. Bright-field images of migration assay performed in Caco-2 cells for 24 and 48 hours in presence of low (5 ng) and high (10 ng) concentrations of rhTSG-6 and quantification of the wound closure respective to time zero. Representative images of 3 independent experiments, with biological triplicates for each group. Data are presented as mean ± SEM. *$P < .05$, **$P < .01$, ***$P < .001$, and **** $P < .0001$ by 1-way analysis of variance, with Tukey's multiple comparisons.

Although further studies are necessary to gain insight into the molecular mechanisms involved, it is reasonable to hypothesize that upon initiation of inflammation the intestinal mucosa responds to damage by synthesizing HA, TSG-6, and other ECM components in an attempt to activate tissue repair. However, pathological HC•HA complex formation impacts the ECM composition and function activating mechanoregulated signaling pathways that lead to the promotion of EMT.[20]

HCs of IαI interact with integrin ligands and thus could modulate the structure of matrix in a variety of ways.[56] Moreover, HC•HA complexes have been found to directly participate in fibroblast to myofibroblast differentiation[64] and may regulate the bioavailability of growth factors involved in these events such as TGFβ.[56] Together, this suggests that in the fistula once the dysfunctional ECM is established, mechanical properties and composition of ECM drive EMT. In turn, EMT sustains changes in the mechanics and composition of the ECM fueling EMT independently of inflammatory processes, thus creating a feedback loop between ECM remodeling and EMT processes. This scenario paves the way for a new management of perianal fistula in CD patients. Indeed, the therapeutic approach may evolve from anti-inflammatory therapies and use of antibiotics to a combination treatment strategy of conventional drugs with regulators of ECM. Although the biological drugs (eg, infliximab and adalimumab) have as primary targets the blocking of the inflammatory cascade, there is evidence they also alter the composition and organization of the ECM[67] by modulating MMPs expression.[68,69] However, these effects on the ECM are rather weak and unspecific and do not take into account the overall changes of ECM mechanical properties. Indeed, a significant proportion of patients only partially respond to these therapies meaning that no single treatment can successfully manage fistula healing. A recent consensus guideline has been designed to simplify the classification of

Figure 5. (*See previous page*). TSG-6 induces Snail and enhances the migratory capacity of Caco-2 cells. (*A*) Relative transcript levels of *TNFAIP6* (which encodes the TSG-6 protein) in control (EV) and TSG-6 OE Caco-2 cells. Data are representative of 3 independent experiments, with biological triplicates for each group. (*B*) Western blot analysis of Caco-2 cells with EV and TSG-6 OE cells. (*C*) Western blot analysis of Caco-2 cell supernatants pretreated with 0.1 M NaOH or with 0.05 U chondroitinase ABC lyase. Shown are that 40 kDa and 150 kDa are the molecular weights expected for TSG-6 free molecules and the complexed TSG-6 forms, respectively. Data are representative of 3 independent experiments, with biological triplicates for each group. (*D*) Expression levels of *CDH1* (which encodes E-cadherin) and *SNAI1* (which encodes Snail) in fistula and perifistula regions from the same patients by RNA-seq analysis (left panel) (n = 8) and qRT-PCR (right panel) (n = 22). (*E*) Relative transcript levels of *CDH1* and *SNAI1* in control (EV) and TSG-6 OE Caco-2 cells. (*F*) [^{3}H]-thymidine–based proliferation assay of control (EV) or TSG-6 OE Caco-2 cells. (*G*) Bright-field images of wound healing assay performed in control or TSG-6 OE Caco-2 cells for 24 and 48 hours, and quantification of the wound closure respective to time zero. Representative images of 3 independent experiments, with biological triplicates for each group. Data are presented as mean ± SEM. *$P < .05$, **$P < .01$, ***$P < .001$, and **** $P < .0001$ by Mann-Whitney test (*A*, *C*, *E*) and 1-way analysis of variance, with Tukey's multiple comparisons (*D*, *G*).

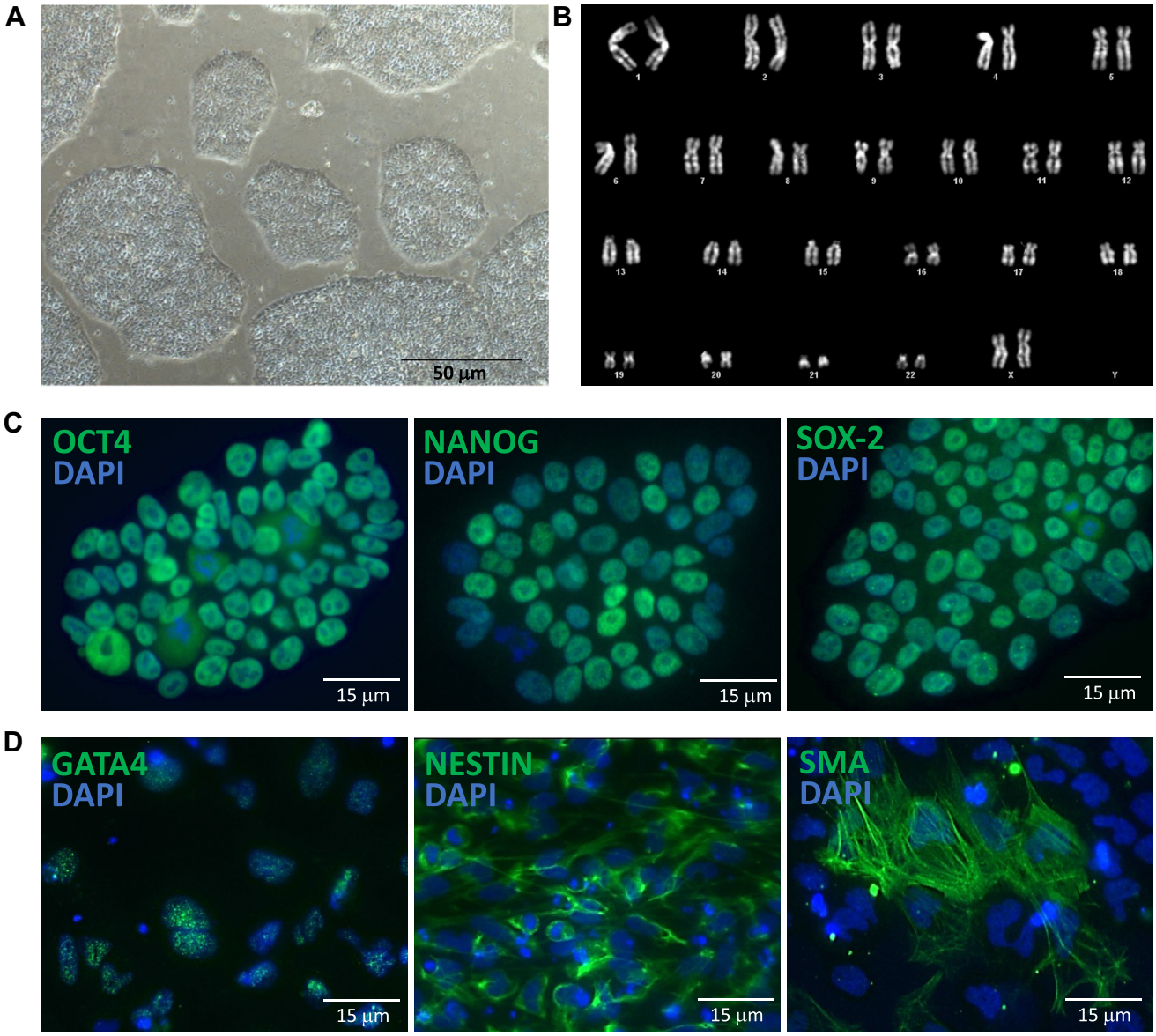

Figure 7. Characterization of HD-iPSCs. (*A*) Representative images of iPSC-like colony morphology of iPSC cells cultured under feeder-free conditions. Scale bar = 50 μm. (*B*) HD-iPSC exhibited a normal diploid karyotype (46,XX). (*C*) Immunostaining for stemness markers (green): OCT4, NANOG, and SOX-2. Scale bar = 15 μm. (*D*) Immunostaining for markers of the 3 germ layers (green): endoderm (GATA4), mesoderm (smooth muscle actin SMA), and ectoderm (NESTIN). Nuclei are counterstained with DAPI (blue). Scale bar = 15 μm.

perianal fistulae and to include proactive medical and surgical approaches.[70] Although there is no histological stratification of the perianal fistula, ECM analysis could inform the choice of combined therapy (ie, to stop ECM-dependent EMT events), and may also allow the design of new strategies for generating antibodies against ECM molecules and using them for novel combined therapies.

Materials and Methods

Surgical Human Tissue Collection

Perianal fistulae involving the anal tract, classified using the Parks criteria based on their relationship to the external and internal anal sphincters, were analyzed in 20 patients diagnosed with CD (Table 1). CD was diagnosed based on clinical, biological, endoscopic, and histological criteria (Crohn's Disease Activity Index score). Surgical specimens from fistula and the nonlesional area named as perifistula, approximately 3 cm from the fistula, were collected from all patients after giving written informed consent. Surgical specimens from healthy mucosa of patients affected from cancer in the upper part of the anus near the rectum were used as a control group [non-IBD] (n = 7). This study was approved by the ethical committee of the Humanitas Clinical and Research Center (no. 2406/2019) and conducted following national and international guidelines.

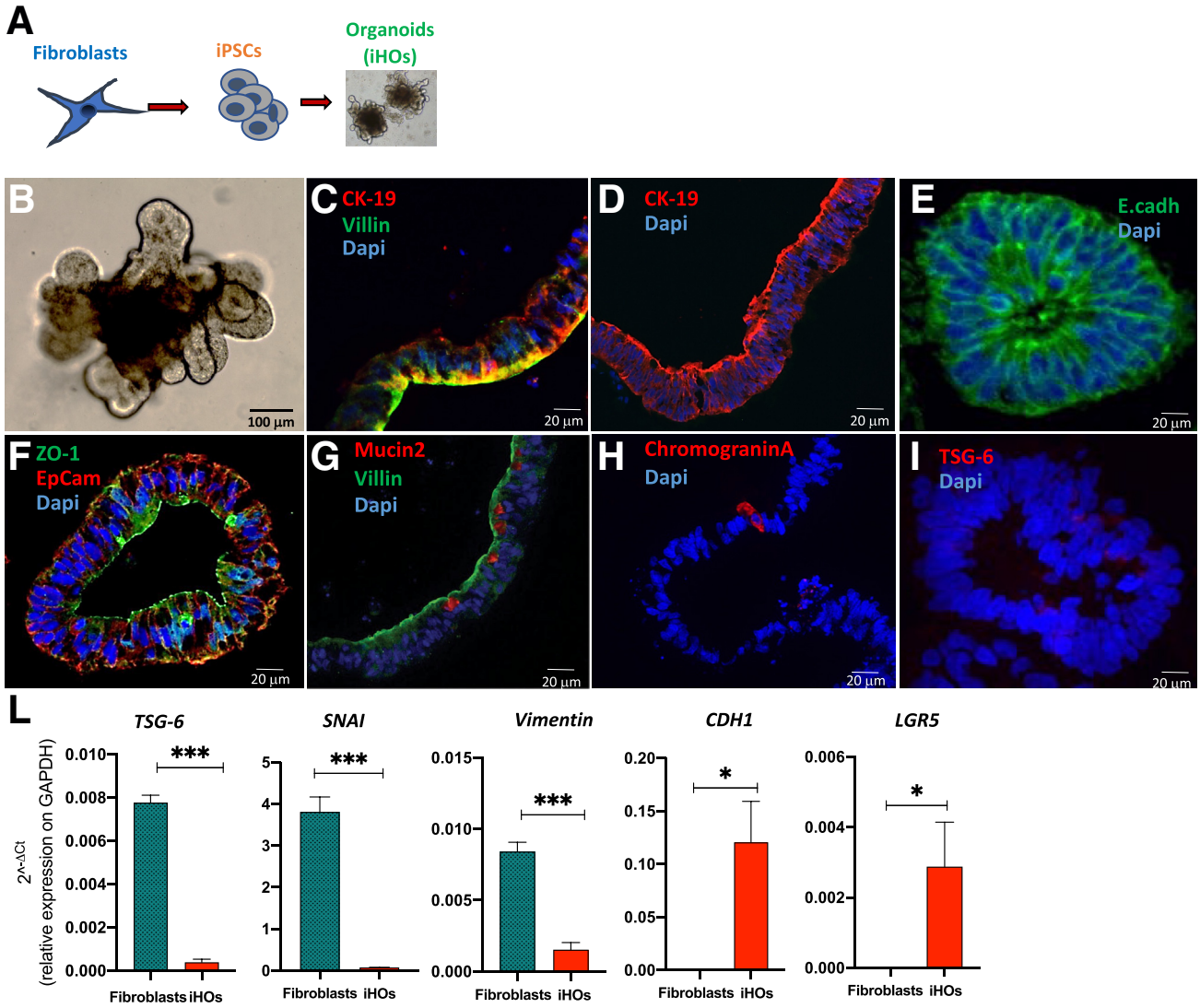

Figure 8. TSG-6 expression in iHOs derived from human dermal iPSCs. (*A*) Schematic reprogramming process of MET, when mesenchymal genes are repressed through the generation of human iPSC-derived iHOs from adult fibroblasts. (*B*) Representative image of cryosection iPSC-derived iHO (*C*, *D*) immunostained for the presence of cytokeratin 19 and villin indicating the presence of a brush border and columnar epithelial cells; (*E–H*) zona occludens-1 and epithelial cellular adhesion molecule indicating the presence of the tight junction facing the lumen of the organoid; villin for enterocytes; anti-mucin-2 indicating the presence of goblet cells; and chromogranin A indicating the presence of enteroendocrine cells; and (*I*) TSG-6. DAPI = nuclei in blue. Scale bars = 100 and 20 μm. (J) Relative transcript levels of *TNFAIP6* encoding for TSG-6, *SNAI1* encoding for Snail, *Vimentin*, *CDH1* encoding E-cadherin, and *LGR5* in fibroblasts and iHOs by qRT-PCR. Data are presented as mean ± SEM. *$P < .05$, ***$P < .001$ by Mann-Whitney test (n = 3).

Cell Culture

The Caco-2 cell line (passages between 18 and 24) (HTB-37; ATCC, Manassas, VA) was cultured in Dulbecco's modified Eagle medium (DMEM) (Gibco, Grand Island, NY) supplemented with 10% (v/v) fetal calf serum (FCS) (EuroClone, Pero, Italy), 1 mmol/L L-glutamine (Lonza, Basel, Switzerland), 1 mmol/L sodium pyruvate (EuroClone), 0.1 mmol/L nonessential amino acids (Lonza), and 100 U/mL antibiotics (penicillin/streptomycin with amphotericin; Lonza) at 37°C in 5% CO_2. Before performing the experiments, the cells were tested for mycoplasma.

Human dermal fibroblasts from a normal donor (Thermo Fisher Scientific, Waltham, MA) were maintained in high-glucose DMEM, supplemented with 10% fetal bovine serum (FBS) (Lonza) at 37°C in humidified air with 5% CO_2.

Human iPSCs were cultured in feeder-free conditions, using StemFlex medium (Thermo Fisher Scientific) on vitronectin-coated 6-well plates (BD Biosciences) at 37°C in humidified air with 5% CO_2.

Isolation of Primary Intestinal Fibroblasts

Surgical specimens were washed with Hank's Balanced Salt Solution (HBSS) (Gibco) containing 10% FCS, 1% antibiotics, and 20 mM HEPES (pH 7.3) (EuroClone) and cut into small pieces. The epithelial layer was removed by

incubating the intestinal fragments with Hepes-buffered HBSS containing 2 mM EDTA solution, at 37°C, for 45 minutes, under gentle agitation. Digestion with HBSS + 5% (v/v) FCS, 5 mM $CaCl_2$, 1 mg/mL collagenase/dispase (Roche, Basel, Switzerland), and 40 μg/mL DNase (Roche Diagnostics) at 37°C for 30 minutes was then performed.

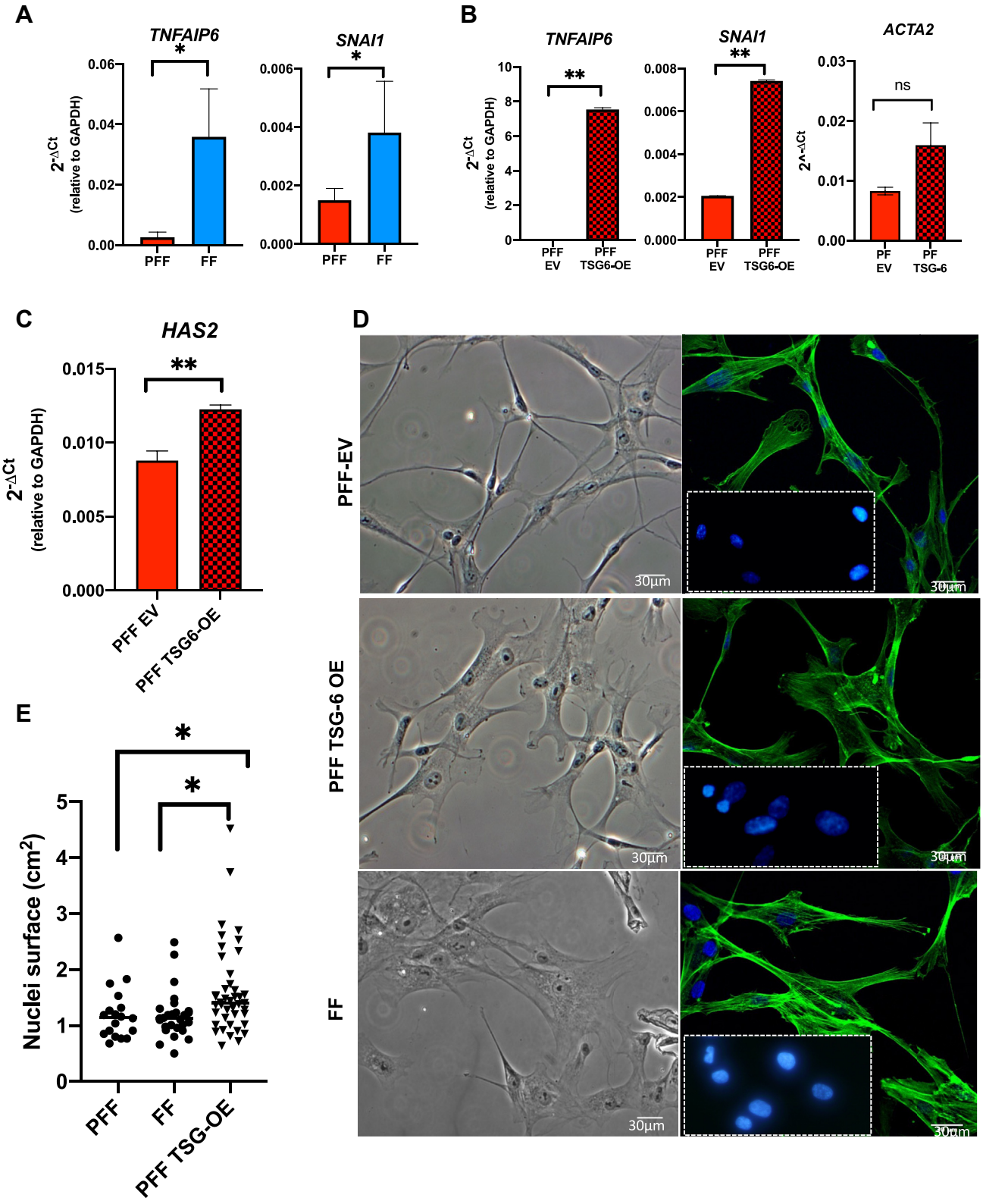

The digested fragments were further disrupted through 100-μm filters (BD falcon) with a 1-mL syringe plunger and washed with 10 mL RPMI medium supplemented with 10% (v/v) FCS and 20 mM Hepes pH 7.3. The single-cell suspension was then filtered through 70-μm filters. Cells were cultured in Gibco M106 supplemented with 10% (v/v) Low Serum Growth Supplement (Thermo Fisher Scientific) and 1% (w/v) antibiotics (penicillin/streptomycin with amphotericin) at 37°C, 5% CO_2, and used between passages 2 and 5. All cell lines were tested for mycoplasma.

Cell Reprogramming

Fibroblasts were reprogrammed by an overnight infection at an multiplicity of infection of 1 in the presence of 4 ng/mL Polybrene (Sigma-Aldrich, St Louis, MO) with a third-generation lentiviral vector described by Sommer et al[71] 19096035 carrying the OCT4, SOX-2, and KLF4 reprogramming factors. The following day, the medium was replaced, and after 48 hours cells were seeded onto mouse embryonic fibroblast feeder layer with ES medium, which was changed daily. iPSC-like colonies were individually picked 4 weeks later and cultured in feeder-free conditions.

Chromosome Preparation and Analysis

Chromosome analysis was done on slide preparations of cells grown on coverslips. Briefly, cell cultures were treated with KaryoMAX Colcemid solution (Thermo Fisher Scientific) at a final concentration of 0.1 μg/mL for 2 hours at 37°C. After hypotonic treatment with 0.075 M KCl and fixation in methanol/acetic acid (3:1 v/v), the slides were air-dried and mounted in Eukitt (Sigma-Aldrich). Chromosome counts and karyotype analyses were done on metaphases stained with VECTASHIELD mounting medium with DAPI (Vector Laboratories, Burlingame, CA) for Q banding.

Images were captured using an Olympus BX61 research microscope (Olympus, Tokyo, Japan) equipped with a cooled charge-coupled device (CCD) camera and analyzed with Applied Imaging software CytoVision (V 4.5.4; master system with mouse karyotyping; CytoVision, Praetoria, South Africa). At least 10 karyotypes were analyzed.

Embryoid Body Formation

Semi-confluent human iPSCs in 1 well of a 6-well plate were dissociated by incubation with 2 mg/mL dispase (STEMCELL Technologies, Vancouver, BC, Canada) at 37°C for 2–3 minutes, or until the colonies began to lift off of the plate. The plates were gently shaken to help dislodge the colonies. The dispase solution was diluted in phosphate-buffered saline (PBS) and the suspension was transferred to a 15-mL centrifuge tube. The cell aggregates were allowed to settle by gravity, and the dispase solution was gently aspirated. The aggregates were washed 3 more times in PBS before being resuspended in 4 mL of Essential 6 medium supplemented with 5 μM Y-27632 ROCK inhibitor. The suspension was gently transferred to each well of a 6-well ultra-low attachment plate (Corning Life Sciences, Acton, MA). After 1 week in suspension, embryoid body formations were transferred to Matrigel-coated dishes and cultured in Essential 6 medium (Thermo Fisher Scientific) for an additional 2–3 weeks. Then, the cells were stained with antibodies against markers of all 3 embryonic germline layers and analyzed by immunofluorescence.

iHO Generation

The differentiation experiments will be performed essentially as described by Lees et al. 2019.[32] Definitive Endoderm differentiation starts by replacing StemFlex medium (Thermo Fisher Scientific) with StemFlex medium supplemented with 10 ng/mL activin A (ActA) and 12 ng/mL basic fibroblast growth factor (bFGF). After 2 days, the medium is replaced with StemFlex medium supplemented with 100 ng/mL ActA, 100 ng/mL bFGF, 10 ng/mL BMP-4, 10 μM LY294002, and 3 μM CHIR99021. The following day, the medium is replaced with RPMI-1640 medium (Lonza) supplemented with 1% serum-free supplement B27 (Thermo Fisher Scientific), 100 ng/mL ActA, and 100 ng/mL bFGF. The differentiation is continued with hindgut induction for 4 days in RPMI/serum-free supplement B27 containing 6 μM CHIR990212 and 3 μM retinoic acid. For 3-dimensional organoid formation, cells will be collected at day 10 and embedded in a small volume of a basement membrane matrix of Matrigel Growth Factor Reduced (BD Biosciences) and seeded into a 60-μL drop/well of 24-well plate. After drop solidification, Advanced DMEM/F12 containing N2 supplement (Thermo Fisher Scientific), B27 serum-free supplement and supplemented with 500 ng/mL R-spondin1, 100 ng/mL noggin, 100 ng/mL epidermal growth factor, 3 μM CHIR990212, 2.5 mM prostaglandin E2, and 10 mM Y-27632 was added. The cytokines and supplements used are shown in Table 1. Medium was changed every 4 days, and organoids was passaged mechanically every 7–10 days. For media change alone Y-27632 was not added; it is only required when seeding/splitting. Organoid cultures was analyzed after 20–30 days in Matrigel Growth Factor Reduced (d30/40 from human HD-iPSCs).

Figure 9. (***See previous page***). **TSG-6 overexpression in PFFs triggers the acquisition of fistula-like features.** (*A*) Relative transcript levels of *TNFAIP6* (which encodes for TSG-6 protein) and *SNAI1* (which encodes for Snail) in PFFs or FFs isolated from the same patient (n = 5). (*B*) Relative transcript levels of *TNFAIP6* and *SNAI1* in PFF control (EV) and overexpressing TSG-6. Data are representative of 2 independent experiments, with biological triplicates for each group (n = 3). (*C*) Relative transcript levels of *HAS2* (encoding for HA synthase 2) and *ACTA2* (encoding for α-smooth muscle actin) in control (EV) or TSG-6 OE perifistula-derived human fibroblasts. (*D*) Bright-field images (left panel) and F-actin immunolabeling (right panel) of human fibroblasts derived from fistula and perifistula areas of the same patient and of perifistula fibroblasts overexpressing TSG-6. Data are representative of 2 independent experiments, with biological triplicates for each group (n = 3). DAPI = nuclei in blue. Scale bar = 30 μm. (*E*) Nuclei surface (cm^2) of human fibroblasts derived was quantified by ImageJ. Data are presented as mean ± SEM. $^*P < .05$, $^{**}P < .01$, and $^{***}P < .001$ by Mann-Whitney test (*A*, *D*, *E*) and 1-way analysis of variance (*F*, *H*).

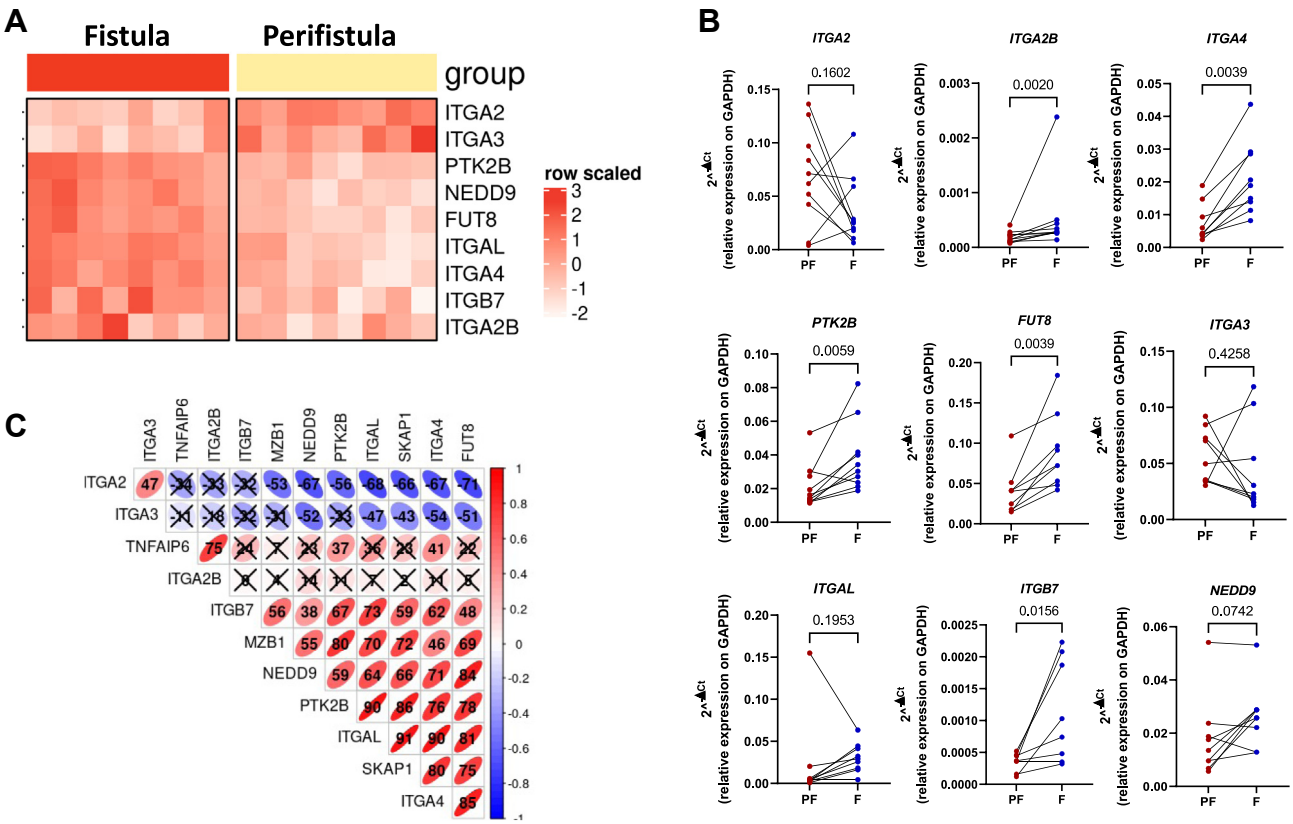

Figure 10. TSG-6 expression in the fistula positively correlates with mediators of mechanotransduction. (*A*) Heatmap representing the expression of genes related to mechanotransduction in fistula and perifistula biopsies. (*B*) Paired analysis of mechanosensitive proteins in fistula and perifistula areas. Gene expression of *ITGA2*, *ITGA2B*, *ITGA4*, *PTK2B*, *FUT8*, *ITGAL*, *ITGB7*, *ITGA3*, and *NEDD9*. For all qRT-PCR results, data reflect mean ± SEM from 3 biological replicates; the results were normalized to *GAPDH* and *P* values were measured by paired *t* test (n = 10 patients for each group). (*C*) Correlation matrix displaying gene-gene Pearson correlation coefficients. Ellipses show gene expression value distributions with red and blue ellipses representing positive and negative correlations, respectively. Cells marked with X represent not significant correlations. n = 8 patients for each group.

Culture of Primary Fibroblasts on Scaffolds

HyStem-C Cell Culture HA scaffold, prepared following the manufacturer's instructions (HYSC010; Sigma-Aldrich), was supplemented with normal human serum (5% v/v) and rhTSG-6 (R&D Systems) at a final concentration of 0.9 μM.[22] Thereafter, PFFs at passage 3 were plated on top of the HA scaffold at a density of 8×10^4 cells/cm^2 and cultured for 24 hours.

Collagen Measurement

Primary fibroblasts were plated in 6-well plates with 2 mL of total medium. Once the cells reached 90% of confluence, cell supernatants were collected by centrifuging at 400 *g* for 5 minutes and stored at −80°C. Total soluble collagen was quantified in cell supernatants determined fluorometrically using the Sircol soluble collagen assay (Biocolor, Newtownabbey, United Kingdom). Collagen was measured as μg/mL based on a set of collagen standards.

Lentiviral Overexpression of TSG-6

The TSG-6 cDNA was cleaved from pCDH_TSG6 (XbaI – BamHI blunted sites),[72] then cloned immediately upstream to the pLenti-C-mGFP (blunted BamHI site) lentiviral vector from OriGene (Rockville, MD). In this vector, the expression of the exogenous cDNA was driven by the cytomegalovirus promoter with the expression of green fluorescent protein. The 2 packaging plasmids psPAX2 and pMD-VSVG were used to produce lentiviral pseudo-particles in HEK 293T cells. Exponentially growing HEK293T cells were transfected with calcium phosphate with the 3-vector lentiviral system. A total of 72 hours after transfection, the supernatant containing the recombinant viruses were collected, filtered (0.45 μm), and centrifuged at 80,000 *g* for 3 hours at 4°C. Then, lentiviral particles were used to infect Caco-2 cells or primary fibroblasts that finally were proceeded to fluorescence-activated cell sorting for sorting green fluorescent protein–positive cells using a BD FACS Melody. Postsorting, the cells were collected in tissue culture medium and plated in T25 cell culture flasks.

Cell Proliferation Assay

Caco-2 cells were infected with lentiviral particles generated with a transfer vector for constitutive

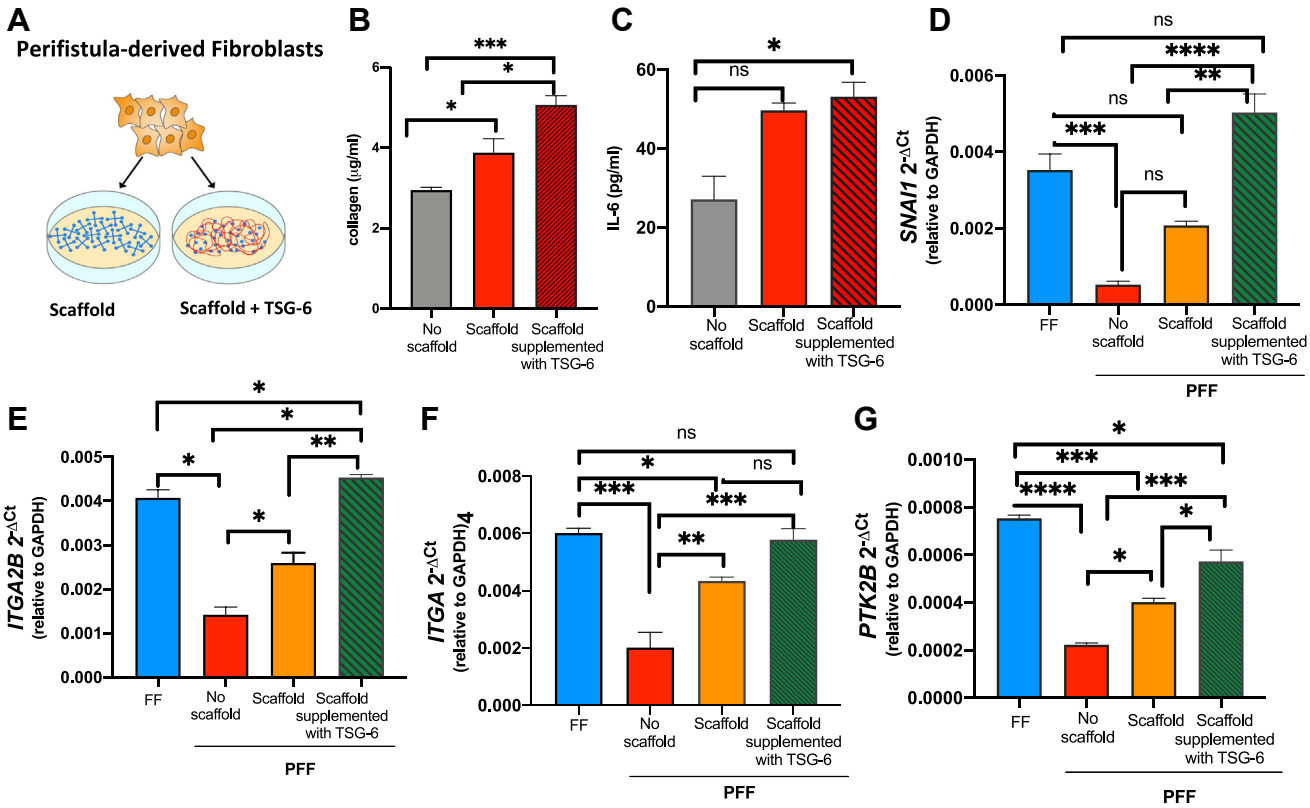

Figure 11. The ECM reorganization mediated by HA•TSG-6 complex promotes the activation of mechanosensors in PFFs. (*A*) Schematic representation of experimental procedure, in which PFFs were plated on HA scaffold ± rhTSG-6. (*B*) Quantification of collagen deposition in PFFs plated on scaffold ± TSG-6. (*C*) IL-6 (pg/mL) levels in PFFs plated on scaffold ± TSG-6. (*D–G*) Relative transcript level of *SNAI1* (encoding for Snail), *ITGA2B* (encoding for integrin alpha 2B), *ITGA4* (encoding for integrin alpha-4), and *PTK2* (encoding for protein tyrosine kinase 2) in FFs vs PFFs plated or not on scaffold ± rhTSG-6. Data are presented as mean ± SEM from 3 independent experiments, with biological triplicates for each group (n = 3). **P* < .05, ***P* < .01, ****P* < .001, and **** *P* < .0001 by 1-way analysis of variance with Tukey's multiple comparison.

overexpression of TSG-6 (Caco-2 TSG-6 OE) or a control empty vector (Caco-2 EV).

Cells were seeded in 96-well plates (5×10^4 cells per well) for 24–48 hours, then were incubated with [^{3}H]-thymidine (PerkinElmer, Waltham, MA) (0.01 mCi/mL) for 16 hours. Cells were harvested at 24 and 48 hours and a scintillation β-counter was used to measure the incorporation of [^{3}H]-thymidine (PerkinElmer). Results were expressed as a percentage of cell proliferation normalized on time zero point.

In Vitro Wound Healing Assay

Wound healing capacity was assessed by a scratch assay on a Caco-2 cell monolayer as previously reported.[73] Briefly, 5×10^4 Caco-2 TSG6-OE or Caco-2 EV were seeded into 24-well culture inserts and incubated at 37°C in a humidified atmosphere with 5% CO_2. After 24 hours, the culture inserts were gently removed using sterile tweezers, and a scratch was made in the monolayers. To evaluate the cells' migratory capacity in the absence of cell proliferation, the cells were preincubated with or without mitomycin C (30 μg/mL; Sigma-Aldrich) for 2h at 37°C. The effects of exogenous TSG-6 on migratory capacity of Caco-2 cells were tested by stimulating the cells with recombinant human TSG-6 (R&D Systems, Minneapolis, MN) (5 ng/well or 10 ng/well). Bright-field images of the wounded area were acquired immediately before stimulation (0 hour time point), and after 24 and 48 hours to monitor the closure of the wounded area, using an inverted microscope (Olympus IX51). The percentage of wound closure was calculated by ImageJ software (ImageJ2 2.3.0; National Institutes of Health, Bethesda, MD) as (Area initial − Area final)/Area initial × 100.

RNA Sequencing and Analysis

Total RNA was extracted from samples using the RNeasy Lipid Tissue Mini kit (Qiagen, Hilden, Germany), according to the manufacturer's instructions. and checked for quality using Tapestation 4200 (Agilent, Santa Clara, CA). RNA-seq libraries were created using the TrueSeq Stranded mRNA Sample Prep Kit (Illumina, San Diego, CA) starting from 400 ng of RNA. Paired-end sequence reads (150 bp in length) were generated on a NextSeq 500 (Illumina). The sequencing reads were processed to remove Illumina barcodes and aligned to the human genome assembly (hg38) using STAR v.2.5.1b with default parameters. FastQ

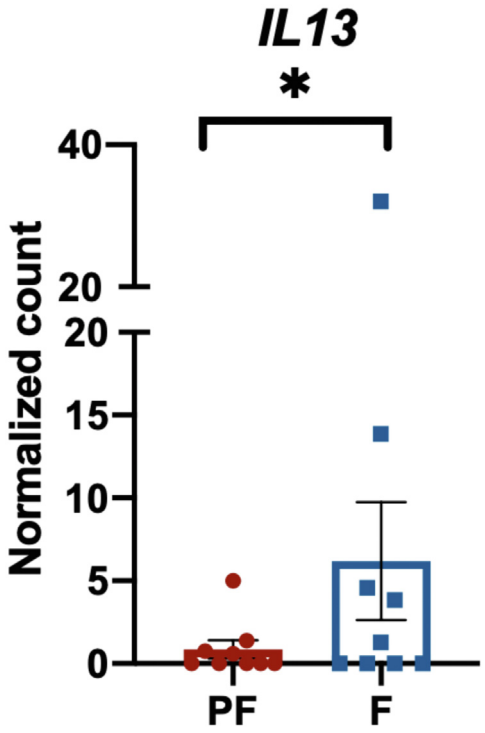

Figure 12. Relative transcript levels of *IL-13* by qRT-PCR. Data are presented as mean ± SEM from 3 biological replicates; the results were normalized to *GAPDH*, and *P* values were measured by paired *t* test (n = 10 patients for each group).

files were mapped to the hg38 human reference genome with the STAR aligner v2.7.3a.[74] Differential gene expression was performed with DESeq2.[75] Functional enrichment was performed with the gene set enrichment analysis and Ingenuity Pathway Analysis (Qiagen). Heatmaps were generated with ComplexHeatmap and multidimensional scaling of transcriptomic data was performed with the rtsne R package by the t-distributed stochastic neighbor embedding machine learning algorithm. Differentially expressed genes were selected based on the following parameters: *P* value $\leq$.05 (upregulation or downregulation). Statistical and downstream bioinformatics analyses were performed within the R environment (R 3.6.3; R Foundation for Statistical Computing, Vienna, Austria). RNA-seq data have been deposited in the National Center for Biotechnology Information Gene Expression Omnibus data repository with the accession number GSE157020. cDNA synthesis was carried out using 1 μg of total RNA with the High Capacity cDNA Reverse Transcription Kit (Applied Biosystems, Bedford, MA). RT-PCR for validation was performed using SYBR Green Master Mix (Applied Biosystems) and detected by using Viia7 Detection system (Applied Biosystems). *GAPDH* was used as a housekeeping gene and the relative abundance was expressed as $2^{-\Delta Ct}$. The specific oligonucleotide primers used are listed in Table 2.

Histological Staining for Collagen Deposition

For histological assessment human samples were fixed in 4% (v/v) formalin, processed, and embedded in paraffin, and 2-μm-thick sections were stained with hematoxylin and eosin.

Collagen deposition was evaluated by Sirius red staining performed on 5-μm-thick formalin-fixed paraffin embedded (FFPE) tissue sections. Second harmonic generation analysis of collagen fibers was conducted by imaging Sirius red–stained slides with the Olympus BX-51 fluorescent microscope using the U-ANT and U-POT polarizers (Olympus), and images were quantified with ImageJ.[76]

Immunofluorescence Staining

On Primary Fibroblasts. Primary fibroblasts seeded on polylysine-coated glass coverslips were fixed in 4% (v/v) paraformaldehyde (PFA) for 10 minutes at room temperature and permeabilized with 0.1% (v/v) Triton X-100 in PBS for 20 minutes at room temperature (all from Sigma-Aldrich). The fixed cells, preincubated for 15 minutes with 1% (w/v) bovine serum albumin, were incubated with Alexa Fluor488-conjugated Phalloidin (F-actin) (1:40; Thermo Fisher Scientific; A12379) for 30 minutes at room temperature. DAPI (1:25,000; Invitrogen) was used for nuclear staining. Coverslips were finally mounted with Fluorescence Mounting Medium (S3023; Dako, Santa Clara, CA). Control slides were obtained by omitting the use of primary antibodies. The images were acquired by Leica SP8 Confocal Microscopy (Leica, Wetzlar, Germany) using 60× objective and analyzed by using ImageJ.

On Human iPSCs, Embryoid Body Formations, and Organoids. Human iPSCs and embryoid body formations were fixed in 4% (v/v) PFA for 10 minutes at room temperature, washed with PBS, and permeabilized in 0.3% Triton X-100 in PBS for 10 minutes at room temperature, whereas intestinal organoids were fixed with 4% PFA, frozen, embedded in Optimal cutting temperature (OCT) compound, and then cut into 10-mm sections and attached to glass slides. Sections were permeabilized in 0.3% Triton X-100 in PBS for 10 minutes at room temperature and blocked in PBS containing 5% FBS for 1 hour before starting the incubation with primary antibodies. Anti-OCT4 (1:200; ab18976; Abcam, Cambridge, United Kingdom), anti-NANOG (1:500; ab62734; Abcam), anti-SOX-2 (1:200; ab97959; Abcam), anti-Nestin (1:200; ab22035; Abcam), anti-α-smooth muscle actin (1:100; ab5694; Abcam), and anti-GATA4 (1:150; ab134057; Abcam). After primary antibody incubation, samples were washed with PBS and incubated with secondary Alexa Fluor 488-conjugated antibodies (Life Technologies, Carlsbad, CA), diluted 1:2000. Samples were also counterstained with DAPI (200 μg/mL). Slides were observed using an Olympus BX61 research microscope equipped with a cooled CCD camera. Images were captured and analyzed with Applied Imaging software CytoVision.

After differentiation, intestinal organoids were fixed with 4% (v/v) PFA, frozen, embedded in OCT compound, and then cut into 10-mm sections and attached to glass slides. Sections were permeabilized in 0.3% Triton X-100 in PBS for 10 minutes at room temperature, blocked in PBS containing 5% FBS for 1 hour, and reacted with the following primary antibodies: anti-chromogranin A (1:250, ab85554;

Abcam), recombinant anti-MUC2 antibody (EPR23479-47) (1:400, ab272692; Abcam), recombinant anti-EpCAM antibody (E144) (1:200, ab32392; Abcam), anti-cytokeratin 19 (1:500 ab7754; Abcam), anti-villin (1.400, ab97512; Abcam), and anti-Zo1 (1:50, 61-7300; Life Technologies) at room temperature for 1 hour. After primary antibody incubation, samples were washed with PBS and incubated at room temperature for 45 minutes with secondary Alexa Fluor 488– or Alexa Fluor 555–conjugated antibodies (1:2000; Life Technologies). Slides were mounted in VECTASHIELD mounting medium with DAPI (Vector Laboratories) and then were observed using an Olympus BX61 research microscope equipped with a cooled CCD camera. Images were captured and analyzed with Applied Imaging software CytoVision.

On Frozen Tissue Sections. Frozen fistula and perifistula sections (4 μm) collected on SuperFrost glass slides (Thermo Fisher Scientific) were fixed in 4% (v/v) PFA for 10 minutes at room temperature and permeabilized with 0.1% (v/v) Triton X-100 in PBS (all from Sigma-Aldrich) for 20 minutes at room temperature. The sections were preincubated for 15 minutes with 1% (w/v) bovine serum albumin, and incubated with anti-IαI antibody (1:50; Dako) overnight at 4°C, followed by incubation for 30 minutes at room temperature with Alexa Fluor 647–conjugated goat anti-rabbit (1:1000; Invitrogen; A21245). Subsequently, fixed tissues were incubated with biotinylated HA binding protein (biotin-HABP; 2.5 μg/mL; HoKuto Co, Nagano, Japan)[77] for 1 hour at room temperature, followed by incubation with Alexa Fluor 488 streptavidin (1:1000; Invitrogen; S32354). DAPI (1:25,000; Invitrogen) was used for nuclear staining. Coverslips were finally mounted with Fluorescence Mounting Medium (Dako; S3023). Control slides were obtained by omitting the use of primary antibodies. The images were acquired by Leica SP8 Confocal Microscopy using 60× objective and analyzed by using ImageJ.

On FFPE Tissue Sections. The 2 μm tissue sections were prepared using standard FFPE fixation and embedding techniques, then antigen retrieval was conducted for 20 minutes at 98°C using Tris EDTA buffer pH = 9. The tissues, preincubated for 1 hour with 2% (w/v) FCS, were incubated with biotin-HABP (2.5 μg/mL; HoKuto Co) and RAH-1 (rabbit anti-human antibody against TSG-6, 1:500 dilution)[78] overnight at 4°C, followed by 30 minutes of incubation at room temperature with Alexa Fluor 488 streptavidin (1:1000; Invitrogen; S32354) and Alexa Fluor 647–conjugated goat anti-rabbit (1:1000; Invitrogen; A21245), respectively. DAPI (1:5000; Invitrogen) was used for nuclear staining. Coverslips were finally mounted with Fluorescence Mounting Medium (Dako; S3023). Control slides were obtained by omitting the use of primary antibodies. The images were acquired by Leica SP8 Confocal Microscopy using a 20× and analyzed by using ImageJ.

Table 1. Clinical Profile of Patients

	CD (n = 22)	Non-IBD (n = 7)
Sex		
Male	16	4
Female	6	3
Age, y	33 (22–62)	45 (20-68)
CD location		
Ileum	13	—
Colon	6	—
Ileocolon	2	—
Rectum	—	7
Upper	1	—
Previous therapies		
Azathioprine	4	—
Infliximab	7	—
Adalimumab	7	—
Vedolizumab	4	—
Systemic corticosteroids	11	—
Smoking status		
Current smoker	8	—
Never smoked	9	—
Past smoker	2	—
Previous surgeries		
Abdominal IBD-related surgeries	9	—
Proctological surgeries	14	—
Familiarity for IBD	4	—

Values are n or median (range).
CD, Crohn's disease; IBD, inflammatory bowel disease.

Western Blot Analysis

Protein extracts from biopsies or cell pellets were solubilized using RIPA buffer—10 mM Tris-HCl (pH 8.0), 1 mM EDTA, 140 mM NaCl, 1% (v/v) Triton X-100, 0.1% (v/v) sodium deoxycholate, 0.1% (w/v) sodium dodecyl sulfate—supplemented with protein inhibitor cocktail (1:50; Thermo Fisher Scientific; A32963). The 30 μg protein extracts were resolved by 8% sodium dodecyl sulfate polyacrylamide gel electrophoresis according to the manufacturer's protocols (Bio-Rad, Hercules, CA). After incubation with 5% (w/v) nonfat milk in Tris-buffered saline with Tween 20 (TBS-T; 10 mM Tris, pH 8.0, 150 mM NaCl, 0.5% (v/v) Tween-20) for 60 minutes, the membranes were incubated with antibodies against TSG-6 (1:1000; RAH-1), or vinculin (1:1000; Santa Cruz Biotechnology, Dallas, TX; sc-25336), or Actin (1:1000; Santa Cruz Biotechnology; sc-1615) overnight at 4°C. Then, after several washes with TBS-T, the membranes were incubated with horseradish peroxidase–conjugated anti-rabbit or anti-mouse antibodies respectively (1:2500; Santa Cruz Biotechnology) for 1 hour at room temperature, followed by development using enhanced chemiluminescence substrate (EuroClone) according to the manufacturer's protocols. Finally, the immunoreactivity was detected by Chemidoc (Bio-Rad) using Quantity One software.

Proteins in the cell culture supernatant were pretreated with 0.1M NaOH for 10 minutes at room temperature (neutralization was performed with 0.1M HCl) or with 0.05 U chondroitinase ABC (Sigma-Aldrich; C2905) for 4 hours at 37°C and concentrated using StrataClean Resin (1:30; Agilent; 400714). Proteins were separated on 10% sodium dodecyl sulfate polyacrylamide gel electrophoresis and transferred onto nitrocellulose membrane according to the manufacturer's protocols (Bio-Rad). After overnight incubation at 4°C with 5% (w/v) nonfat milk in TBS-T, the membranes were incubated with the antibody against TSG-6 (ap_RAH-2 rabbit anti-human

Table 2. List of Real-Time Polymerase Chain Reaction Primers

Gene	Forward	Reverse
TNFAIP6	5′ TTTCTCTTGCTATGGGAAGACAC 3′	5′ GAGCTTGTATTTGCCAGACCG 3′
CDH1	5′ CGAGAGCTACACGTTCACGG 3′	5′ GGGTGTCGAGGGAAAAATAGG 3′
CD44	5′ CTGCCGCTTTGCAGGTGTA 3′	5′ CATTGTGGGCAAGGTGCTATT 3′
IL6	5′ACTCACCTCTTCAGAACGAATTG 3′	5′ CCATCTTTGGAAGGTTCAGGTTG 3′
HAS1	5′ GAGCCTCTTCGCGTACCTG 3′	5′ CCTCCTGGTAGGCGGAGAT 3′
HAS2	5′ CTCTTTTGGACTGTATGGTGCC 3′	5′ AGGGTAGGTTAGCCTTTTCACA 3′
ITGA2	5′ ACAAGCGTTACTGTGAAGCG 3′	5′ GGGCCAGGAGACCTAAGAAATAA 3′
ITGA2B	5′ CACCTCAGCATCCACCTTCCG 3′	5′ GTCTGCGATCCCGCTTGTGATG 3′
ITGA4	5′ CACAACACGCTGTTCGGCTA 3′	5′ CGATCCTGCATCTGTAAATCGC 3′
PTK2B	5′ CCCCTGAGTCGAGTAAAGTTGG 3′	5′ GATACGCACGTCCTCCTTTTC 3′
SNAI1	5′ TCGGAAGCCTAACTACAGCGA 3′	5′ AGATGAGCATTGGCAGCGAG 3′
TNFalpha	5′ CCTCTCTCTAATCAGCCCTCTG 3′	5′ GAGGACCTGGGAGTAGATGAG 3′
GAPDH	5′ GGAGCGAGATCCCTCCAAAAT 3′	5′ GGCTGTTGTCATACTTCTCATGG 3′
ACTA2	5′ ACTGCCTTGGTGTGTGACAA 3′	5′ TCCCAGTTGGTGATGATGCC 3′
FUT8	5′ GGTGGATGGGAGACTGTATTT 3′	5′ GTCTTCTGGTACAGCCAAGGGT 3′
ITGA3	5′ TGTGGCTTGGAGTGACTGTG 3′	5′ TCATTGCCTCGCACGTAGC 3′
ITGAL	5′ CGTGGTGTATGAGAAGCAGATG 3′	5′ GCTCAGAGTCTTCTGCAGGGAT 3′
ITGB7	5′ CAGCTTTCACCATGTGCTGTC 3′	5′ CCAGCAGCCGGGACACATTT 3′
NEDD9	5′ GGAGGAGTTTGAGAGGCAACA 3′	5′ CTCACGCCACTGTTTGTGGT 3′
MMP9	5′ TGTACCGCTATGGTTACACTCG 3′	5′ GGCAGGGACAGTTGCTTCT 3′
MMP13	5′ GTTTGGTCCGATGTAACTCCTCT 3′	5′ CATCTCCTCCATAATTTGGC 3′
MMP19	5′ CTGCTGTCTACTCGCCTCGA 3′	5′ GAGAGGCCAATAGAGAGCTG 3′
MMP25	5′ CCTCGGCGCAGGACGTGA 3′	5′ GCGAACCTCTGCATGACTTTG 3′
LGR5	5′ GAGTTACGTCTTGCGGGAAAC 3′	5′TGGGTACGTGTCTTAGCTGATTA 3′
VIMENTIN	5′GGACCAGCTAACCAACGACA 3′	5′ AAGGTCAAGACGTGCCAGAG 3′

antibody 1:800) overnight at 4°C. The rabbit anti-human antibody RAH-2 was affinity purified (ap) by incubation with the peptide CTSTGNKNFLAGRFSHL (used for immunization), immobilized via the N-terminal cysteine to SulfoLink Coupling Resin (Thermo Fisher Scientific), where bound IgG was eluted at pH 2 and concentrated with buffer exchange into PBS. Then, membranes were incubated with horseradish peroxidase–conjugated anti-rabbit (1:1000; Santa Cruz Biotechnology) for 1 hour at room temperature. The development and the detection of the immunoreactivity were performed as reported previously.

Statistical Analysis

Statistical analyses were performed with GraphPad Prism version 8 (GraphPad Software, San Diego, CA) using Student *t* test or Mann-Whitney *U* test for the comparison between 2 groups, whereas 1-way or 2-way analysis of variance with Bonferroni posttest analysis was used for the comparison of multiple groups and paired Student *t* tests for comparisons between 2 means. The data were expressed as mean ± SEM. Statistical significance was defined as $P < .05$.

References

1. Torres J, Mehandru S, Colombel JF, et al. Crohn's disease. Lancet 2017;389:1741–1755.
2. Roda G, Chien Ng S, Kotze PG, et al. Crohn's disease. Nat Rev Dis Primers 2020;6:22.
3. Gecse KB, Bemelman W, Kamm MA, et al. A global consensus on the classification, diagnosis and multidisciplinary treatment of perianal fistulising Crohn's disease. Gut 2014;63:1381–1392.
4. Beaugerie L, Seksik P, Nion-Larmurier I, et al. Predictors of Crohn's disease. Gastroenterology 2006;130:650–656.
5. Bell SJ, Williams AB, Wiesel P, et al. The clinical course of fistulating Crohn's disease. Aliment Pharmacol Ther 2003;17:1145–1151.
6. Marzo M, Felice C, Pugliese D, et al. Management of perianal fistulas in Crohn's disease: an up-to-date review. World J Gastroenterol 2015;21:1394–1403.
7. Wasmann KA, de Groof EJ, Stellingwerf ME, et al. Treatment of perianal fistulas in Crohn's disease, seton versus anti-TNF versus surgical closure following anti-TNF [PISA]: a randomised controlled trial. J Crohns Colitis 2020;14:1049–1056.
8. Scharl M, Rogler G. Pathophysiology of fistula formation in Crohn's disease. World J Gastrointest Pathophysiol 2014;5:205–212.
9. Leeb SN, Vogl D, Gunckel M, et al. Reduced migration of fibroblasts in inflammatory bowel disease: role of inflammatory mediators and focal adhesion kinase. Gastroenterology 2003;125:1341–1354.

10. Meier JK, Scharl M, Miller SN, et al. Specific differences in migratory function of myofibroblasts isolated from Crohn's disease fistulae and strictures. Inflamm Bowel Dis 2011;17:202–212.
11. Flier SN, Tanjore H, Kokkotou EG, et al. Identification of epithelial to mesenchymal transition as a novel source of fibroblasts in intestinal fibrosis. J Biol Chem 2010; 285:20202–20212.
12. Bataille F, Rohrmeier C, Bates R, et al. Evidence for a role of epithelial–mesenchymal transition during pathogenesis of fistulae in Crohn's disease. Inflamm Bowel Dis 2008;14:1514–1527.
13. Scharl M, Weber A, Furst A, et al. Potential role for SNAIL family transcription factors in the etiology of Crohn's disease-associated fistulae. Inflamm Bowel Dis 2011; 17:1907–1916.
14. Scharl M, Huber N, Lang S, et al. Hallmarks of epithelial to mesenchymal transition are detectable in Crohn's disease associated intestinal fibrosis. Clin Transl Med 2015;4:1.
15. Lovisa S, Genovese G, Danese S. Role of epithelial-to-mesenchymal transition in inflammatory bowel disease. J Crohns Colitis 2019;13:659–668.
16. Ortiz-Masia D, Salvador P, Macias-Ceja DC, et al. WNT2b activates epithelial-mesenchymal transition through FZD4: relevance in penetrating Crohn s disease. J Crohns Colitis 2020;14:230–239.
17. Kirkegaard T, Hansen A, Bruun E, et al. Expression and localisation of matrix metalloproteinases and their natural inhibitors in fistulae of patients with Crohn's disease. Gut 2004;53:701–709.
18. Frantz C, Stewart KM, Weaver VM. The extracellular matrix at a glance. J Cell Sci 2010;123:4195–4200.
19. Wang A, de la Motte C, Lauer M, et al. Hyaluronan matrices in pathobiological processes. FEBS J 2011; 278:1412–1418.
20. Scott LE, Weinberg SH, Lemmon CA. Mechanochemical signaling of the extracellular matrix in epithelial-mesenchymal transition. Front Cell Dev Biol 2019;7:135.
21. Day AJ, Milner CM. TSG-6: A multifunctional protein with anti-inflammatory and tissue-protective properties. Matrix Biol 2019;78–79:60–83.
22. Romano B, Elangovan S, Erreni M, et al. TNF-stimulated gene-6 is a key regulator in switching stemness and biological properties of mesenchymal stem cells. Stem Cells 2019;37:973–987.
23. Szendroi M, Vajta G, Kovacs L, et al. Polarization colours of collagen fibres: a sign of collagen production activity in fibrotic processes. Acta Morphol Hung 1984; 32:47–55.
24. Naba A, Clauser KR, Ding H, et al. The extracellular matrix: tools and insights for the "omics" era. Matrix Biol 2016;49:10–24.
25. Zhuo L, Kanamori A, Kannagi R, et al. SHAP potentiates the CD44-mediated leukocyte adhesion to the hyaluronan substratum. J Biol Chem 2006;281:20303–20314.
26. Tseng SC. HC-HA/PTX3 purified from amniotic membrane as novel regenerative matrix: insight into relationship between inflammation and regeneration. Invest Ophthalmol Vis Sci 2016;57:ORSFh1–ORSFh18.
27. Lord MS, Melrose J, Day AJ, et al. The inter-alpha-trypsin inhibitor family: versatile molecules in biology and pathology. J Histochem Cytochem 2020;68:907–927.
28. de la Motte CA, Hascall VC, Drazba J, et al. Mononuclear leukocytes bind to specific hyaluronan structures on colon mucosal smooth muscle cells treated with polyinosinic acid:polycytidylic acid: inter-alpha-trypsin inhibitor is crucial to structure and function. Am J Pathol 2003;163:121–133.
29. Bommaya G, Meran S, Krupa A, et al. Tumour necrosis factor-stimulated gene (TSG)-6 controls epithelial-mesenchymal transition of proximal tubular epithelial cells. Int J Biochem Cell Biol 2011;43:1739–1746.
30. Paulis M, Susani L, Castelli A, et al. Chromosome transplantation: a possible approach to treat human X-linked disorders. Mol Ther Methods Clin Dev 2020; 17:369–377.
31. Sommer CA, Stadtfeld M, Murphy GJ, et al. Induced pluripotent stem cell generation using a single lentiviral stem cell cassette. Stem Cells 2009;27:543–549.
32. Lees EA, Forbester JL, Forrest S, et al. Using human induced pluripotent stem cell-derived intestinal organoids to study and modify epithelial cell protection against Salmonella and other pathogens. J Vis Exp 2019.
33. Jansen KA, Atherton P, Ballestrem C. Mechanotransduction at the cell-matrix interface. Semin Cell Dev Biol 2017;71:75–83.
34. Baranova NS, Nileback E, Haller FM, et al. The inflammation-associated protein TSG-6 cross-links hyaluronan via hyaluronan-induced TSG-6 oligomers. J Biol Chem 2011;286:25675–25686.
35. O'Reilly S, Ciechomska M, Cant R, et al. Interleukin-6 (IL-6) trans signaling drives a STAT3-dependent pathway that leads to hyperactive transforming growth factor-beta (TGF-beta) signaling promoting SMAD3 activation and fibrosis via GremLin protein. J Biol Chem 2014; 289:9952–9960.
36. Lovisa S. Epithelial-to-mesenchymal transition in fibrosis: concepts and targeting strategies. Front Pharmacol 2021;12:737570.
37. Brabletz T, Kalluri R, Nieto MA, et al. EMT in cancer. Nat Rev Cancer 2018;18:128–134.
38. Ricard-Blum S. The collagen family. Cold Spring Harb Perspect Biol 2011;3:a004978.
39. Petrey AC, de la Motte CA. Hyaluronan, a crucial regulator of inflammation. Front Immunol 2014;5:101.
40. Muncie JM, Weaver VM. The physical and biochemical properties of the extracellular matrix regulate cell fate. Curr Top Dev Biol 2018;130:1–37.
41. Petrey AC, de la Motte CA. Hyaluronan in inflammatory bowel disease: Cross-linking inflammation and coagulation. Matrix Biol 2019;78–79:314–323.
42. Donlan AN, Sutherland TE, Marie C, et al. IL-13 is a driver of COVID-19 severity. JCI Insight 2021;6:e150107.
43. Bell TJ, Brand OJ, Morgan DJ, et al. Defective lung function following influenza virus is due to prolonged, reversible hyaluronan synthesis. Matrix Biol 2019;80:14–28.
44. Milner CM, Day AJ. TSG-6: a multifunctional protein associated with inflammation. J Cell Sci 2003; 116:1863–1873.

45. Milner CM, Higman VA, Day AJ. TSG-6: a pluripotent inflammatory mediator? Biochem Soc Trans 2006; 34:446–450.
46. Sala E, Genua M, Petti L, et al. Mesenchymal stem cells reduce colitis in mice via release of TSG6, independently of their localization to the intestine. Gastroenterology 2015;149:163–176.e20.
47. Song WJ, Li Q, Ryu MO, et al. TSG-6 secreted by human adipose tissue-derived mesenchymal stem cells ameliorates DSS-induced colitis by inducing M2 macrophage polarization in mice. Sci Rep 2017;7:5187.
48. Di G, Du X, Qi X, et al. Mesenchymal stem cells promote diabetic corneal epithelial wound healing through TSG-6-dependent stem cell activation and macrophage switch. Invest Ophthalmol Vis Sci 2017;58:4344–4354.
49. Gesteira TF, Sun M, Coulson-Thomas YM, et al. Hyaluronan rich microenvironment in the limbal stem cell niche regulates limbal stem cell differentiation. Invest Ophthalmol Vis Sci 2017;58:4407–4421.
50. Oh JY, Roddy GW, Choi H, et al. Anti-inflammatory protein TSG-6 reduces inflammatory damage to the cornea following chemical and mechanical injury. Proc Natl Acad Sci U S A 2010;107:16875–16880.
51. Qi Y, Jiang D, Sindrilaru A, et al. TSG-6 released from intradermally injected mesenchymal stem cells accelerates wound healing and reduces tissue fibrosis in murine full-thickness skin wounds. J Invest Dermatol 2014; 134:526–537.
52. Sammarco G, Shalaby M, Elangovan S, et al. Hyaluronan accelerates intestinal mucosal healing through interaction with TSG-6. Cells 2019;8:1074.
53. Rugg MS, Willis AC, Mukhopadhyay D, et al. Characterization of complexes formed between TSG-6 and inter-alpha-inhibitor that act as intermediates in the covalent transfer of heavy chains onto hyaluronan. J Biol Chem 2005;280:25674–25686.
54. Briggs DC, Birchenough HL, Ali T, et al. Metal ion-dependent heavy chain transfer activity of TSG-6 mediates assembly of the cumulus-oocyte matrix. J Biol Chem 2015;290:28708–28723.
55. Sivakumar A, Mahadevan A, Lauer ME, et al. Midgut laterality is driven by hyaluronan on the right. Dev Cell 2018;46:533–551.e5.
56. Briggs DC, Langford-Smith AWW, Birchenough HL, et al. Inter-alpha-inhibitor heavy chain-1 has an integrin-like 3D structure mediating immune regulatory activities and matrix stabilization during ovulation. J Biol Chem 2020;295:5278–5291.
57. Baranova NS, Inforzato A, Briggs DC, et al. Incorporation of pentraxin 3 into hyaluronan matrices is tightly regulated and promotes matrix cross-linking. J Biol Chem 2014;289:30481–30498.
58. Matuska B, Comhair S, Farver C, et al. Pathological hyaluronan matrices in cystic fibrosis airways and secretions. Am J Respir Cell Mol Biol 2016;55:576–585.
59. Stober VP, Johnson CG, Majors A, et al. TNF-stimulated gene 6 promotes formation of hyaluronan-inter-alpha-inhibitor heavy chain complexes necessary for ozone-induced airway hyperresponsiveness. J Biol Chem 2017;292:20845–20858.
60. Baranova NS, Foulcer SJ, Briggs DC, et al. Inter-alpha-inhibitor impairs TSG-6-induced hyaluronan cross-linking. J Biol Chem 2013;288:29642–29653.
61. Lesley J, Gal I, Mahoney DJ, et al. TSG-6 modulates the interaction between hyaluronan and cell surface CD44. J Biol Chem 2004;279:25745–25754.
62. Choi H, Lee RH, Bazhanov N, et al. Anti-inflammatory protein TSG-6 secreted by activated MSCs attenuates zymosan-induced mouse peritonitis by decreasing TLR2/NF-kappaB signaling in resident macrophages. Blood 2011;118:330–338.
63. Kota DJ, Wiggins LL, Yoon N, et al. TSG-6 produced by hMSCs delays the onset of autoimmune diabetes by suppressing Th1 development and enhancing tolerogenicity. Diabetes 2013;62:2048–2058.
64. Martin J, Midgley A, Meran S, et al. Tumor necrosis factor-stimulated gene 6 (TSG-6)-mediated interactions with the inter-alpha-inhibitor heavy chain 5 facilitate tumor growth factor beta1 (TGFbeta1)-dependent fibroblast to myofibroblast differentiation. J Biol Chem 2016;291:13789–13801.
65. Watanabe R, Watanabe H, Takahashi Y, et al. Atheroprotective effects of tumor necrosis factor-stimulated gene-6. J Am Coll Cardiol Basic Trans Science 2016; 1:494–509.
66. Zhao XK, Cheng Y, Liang Cheng M, et al. Focal adhesion kinase regulates fibroblast migration via integrin beta-1 and plays a central role in fibrosis. Sci Rep 2016;6:19276.
67. Sorrentino D, Terrosu G, Vadala S, et al. Fibrotic strictures and anti-TNF-alpha therapy in Crohn‘s disease. Digestion 2007;75:22–24.
68. Wendling D, Cedoz JP, Racadot E. Serum levels of MMP-3 and cathepsin K in patients with ankylosing spondylitis: effect of TNFalpha antagonist therapy. Joint Bone Spine 2008;75:559–562.
69. Di Sabatino A, Saarialho-Kere U, Buckley MG, et al. Stromelysin-1 and macrophage metalloelastase expression in the intestinal mucosa of Crohn‘s disease patients treated with infliximab. Eur J Gastroenterol Hepatol 2009;21:1049–1055.
70. Geldof J, Iqbal N, LeBlanc JF, et al. Classifying perianal fistulising Crohn‘s disease: an expert consensus to guide decision-making in daily practice and clinical trials. Lancet Gastroenterol Hepatol 2022;7:576–584.
71. Sommer CA, Stadtfeld M, Murphy GJ, Hochedlinger K, Kotton DN, Mostoslavsky G. Induced pluripotent stem cell generation using a single lentiviral stem cell cassette. Stem Cells 2009 Mar;27(3):543–549.
72. Drummond SP, Bartnik E, Kouvatsos N, et al. The recombinant Link module of human TSG-6 suppresses cartilage damage in models of osteoarthritis: a potential disease-modifying OA drug. medRxiv https://doi.org/10.1101/2021.03.23.21254102.
73. Vetrano S, Ploplis VA, Sala E, et al. Unexpected role of anticoagulant protein C in controlling epithelial barrier integrity and intestinal inflammation. Proc Natl Acad Sci U S A 2011;108:19830–19835.
74. Dobin A, Davis CA, Schlesinger F, et al. STAR: ultrafast universal RNA-seq aligner. Bioinformatics 2013;29:15–21.
75. Love MI, Huber W, Anders S. Moderated estimation of fold change and dispersion for RNA-seq data with DESeq2. Genome Biol 2014;15:550.

76. Chen Y, Yu Q, Xu C-B. A convenient method for quantifying collagen fibers in atherosclerotic lesions by ImageJ software. Int J Clin Exp Med 2017; 10:14904–14910.
77. Clark SJ, Keenan TD, Fielder HL, et al. Mapping the differential distribution of glycosaminoglycans in the adult human retina, choroid, and sclera. Invest Ophthalmol Vis Sci 2011;52:6511–6521.
78. Fujimoto T, Savani RC, Watari M, et al. Induction of the hyaluronic acid-binding protein, tumor necrosis factor-stimulated gene-6, in cervical smooth muscle cells by tumor necrosis factor-alpha and prostaglandin E(2). Am J Pathol 2002;160:1495–1502.

Received May 26, 2022. Accepted December 7, 2022.

Correspondence
Address correspondence to: Stefania Vetrano, PhD, Department of Biomedical Sciences, Humanitas University, Via Rita Levi Montalcini, 20090, Pieve Emanuele (Milan) Italy. e-mail: stefania.vetrano@hunimed.eu.

CRediT Authorship Contributions

Federica Rubbino, PhD (Formal analysis: Equal; Funding acquisition: Equal; Methodology: Equal; Writing – original draft: equal; Writing – review & editing: Equal)

Giulia Rizzo, Dr (Conceptualization: lead;Formal analysis: Equal; Methodology: Equal; Validation: Lead; Writing – original draft: lead; review & editing: Equal)

Sudharshan Elangovan, PhD (Conceptualization: Lead; Funding acquisition: Equal; Methodology: Lead; Writing – original draft: Supporting)

Giusy Sammarco, Dr (Methodology: Supporting)

Sara Lovisa, PhD (Formal analysis: Supporting; Funding acquisition: Equal; Validation: Supporting; Writing – original draft: Equal; Writing – review & editing: Equal)

Restelli Silvia, Dr (Methodology: Lead)

Samuel Pineda Chavez, Dr (Methodology: Supporting)

Luca Massimino, PhD (Formal analysis: Equal)

Luigi Lamparelli, Dr (Formal analysis: Supporting)

Marianna Paulis (Methodology: Supporting)

Annalisa Maroli, MD (Resources: Equal)

Giulia Roda, MD (Resources: Supporting)

Mohammad Shalaby, Dr (Methodology: Supporting)

Michele Carvello, MD (Resources: Equal)

Caterina Foppa, MD (Resources: Supporting)

Sheona P. Drummond, PhD (Resources: Supporting; Writing – review & editing: Equal)

Paola Spaggiari, Dr (Resources: Supporting)

Federica Ungaro, PhD (Writing – review & editing: Supporting)

Antonino Spinelli, MD (Resources: Equal)

Alberto Malesci, MD (Writing – original draft: Supporting; Writing – review & editing: Supporting)

Alessandro Repici, MD (Resources: Lead)

Anthony J. Day, MA (Resources: Supporting; Writing – review & editing: Lead)

Alessandro Armuzzi, MD (Writing – review & editing: Equal)

Silvio Danese, MD (Supervision: Supporting)

Stefania Vetrano, PhD (Conceptualization: Lead; Formal analysis: Equal; Funding acquisition: lead; Supervision: Lead; Visualization: Lead; Writing – original draft: Lead Writing – review & editing: Lead)

Conflicts of Interest

These authors disclose the following: Anthony J. Day is a founder and shareholder of Link Biologics Ltd, which is focused on the development of TSG-6–based protein biological drug. Silvio Danese has served as speaker, consultant, and advisory board member for Shering-Plough, Abbott Laboratories, Merck and Co, UCB Pharma, Ferring, Cellerix, Millennium Takeda, Nycomed, Pharmacosmos, Actelion, Alfa Wasserman, Genentech, Pfizer, AstraZeneca, Novo Nordisk, Cosmo Pharmaceuticals, Vifor, and Johnson and Johnson. The remaining authors disclose no conflicts.

Funding

This research was supported by a European Crohn's and Colitis Organisation fellowship (to Sudharshan Elangovan), an AIRC fellowship (project code 25484) (to Federica Rubbino), a Fondazione Umberto Veronesi Fellowship (to Sara Lovisa), the European Union's Horizon 2020 research and innovator program under Marie Sklodowska-Curie grant agreement #101029427 (to Sara Lovisa), Esprinet SpA Italy (to Stefania Vetrano and Giulia Rizzo), Versus Arthritis funding for generation of the pCDH_TSG6 construct and ap_RAH-2 antibody (grants 20895 and 22277) (to Anthony J. Day), and the GP/EFSA/SCER/2020/03 (Lot 2 exploring the use of gut-on-a-chip models) project (to Marianna Paulis).